Observations of River Plume Mixing in the Surf Zone

S. E. KASTNER,[a] A. R. HORNER-DEVINE,[b] J. M. THOMSON,[c] AND S. N. GIDDINGS[d]

[a] *Department of Environmental Science, Western Washington University, Bellingham, Washington*
[b] *Department of Civil and Environmental Engineering, University of Washington, Seattle, Washington*
[c] *Applied Physics Laboratory, University of Washington, Seattle, Washington*
[d] *Scripps Institution of Oceanography, University of California, San Diego, La Jolla, California*

(Manuscript received 3 December 2021, in final form 14 October 2022)

ABSTRACT: We use salinity observations from drifters and moorings at the Quinault River mouth to investigate mixing and stratification in a surf-zone-trapped river plume. We quantify mixing based on the rate of change of salinity DS/Dt in the drifters' quasi-Lagrangian reference frame. We estimate a constant value of the vertical eddy diffusivity of salt of $K_z = (2.2 \pm 0.6) \times 10^{-3}$ m^2 s^{-1}, based on the relationship between vertically integrated DS/Dt and stratification, with values as high as 1×10^{-2} m^2 s^{-1} when stratification is low. Mixing, quantified as DS/Dt, is directly correlated to surf-zone stratification, and is therefore modulated by changes in stratification caused by tidal variability in freshwater volume flux. High DS/Dt is observed when the near-surface stratification is high and salinity gradients are collocated with wave-breaking turbulence. We observe a transition from low stratification and low DS/Dt at low tidal stage to high stratification and high DS/Dt at high tidal stage. Observed wave-breaking turbulence does not change significantly with stratification, tidal stage, or offshore wave height; as a result, we observe no relationship between plume mixing and offshore wave height for the range of conditions sampled. Thus, plume mixing in the surf zone is altered by changes in stratification; these are due to tidal variability in freshwater flux from the river and not wave conditions, presumably because depth-limited wave breaking causes sufficient turbulence for mixing to occur during all observed conditions.

SIGNIFICANCE STATEMENT: River outflows are important sources of pollutants, sediment, and nutrients to the coastal ocean. Small rivers often meet large breaking waves in the surf zone close to shore, trapping river water and river-borne material near the beach. Such trapped material can influence coastal public health, beach morphology, and nearshore ecology. This study investigates how trapped fresh river water mixes with salty ocean water in the presence of large breaking waves by using high-resolution measurements of waves, salinity, and turbulence. We find that the surf zone is often fresh and stratified, which could have significant implications for the fate of riverine material. Wave breaking provides a constant source of turbulence, and the amount of mixing is limited by the degree of vertical salt stratification; more mixing occurs when stratification is higher.

KEYWORDS: Estuaries; Rivers; Coastal flows; Mixing; Wave breaking

1. Introduction

Riverine transport of freshwater, nutrients, sediment, and pollutants is important to coastal environments (Hickey et al. 2010). Small discharge rivers represent a large fraction of total river discharge in the midlatitudes (Izett and Fennel 2018), and many such rivers empty directly into the surf zone, where surface waves break near shore due to depth limitation. Recent work predicts the quantity of river water that escapes the surf zone, finding that river discharge is often trapped in the surf zone (Wong et al. 2013; Rodriguez et al. 2018; Kastner et al. 2019). This study uses observational data, including salinity measurements from Lagrangian drifters, from near the Quinault River mouth to investigate transport and mixing in a surf-zone-trapped river plume.

a. Mixing in river plumes

River plumes are frequently approximated as two-layer flows (Fong and Geyer 2001; Hetland 2010; McCabe et al. 2008; Kastner et al. 2018) in which stratification and shear are highest near the base of the plume layer, resulting in the collocation of turbulence and the salinity gradient. Vertical mixing in river plumes is typically driven by stratified shear instabilities along this interface, which occur when vertical shear is strong enough to overcome stratification (MacDonald and Geyer 2004; Geyer et al. 2010; MacDonald et al. 2007; Kilcher et al. 2012; Jurisa et al. 2016). The associated turbulent kinetic energy (TKE) dissipation values in river plumes are typically $\varepsilon \sim O(\text{from } 10^{-8} \text{ to } 10^{-3})$ W kg^{-1} (Nash and Moum 2005; MacDonald et al. 2007; Kilcher et al. 2012; Jurisa et al. 2016). River plume mixing has been shown to be predominantly a vertical process; lateral mixing in river plumes is small because the aspect ratio of a river plume is typically small (MacDonald and Geyer 2004; Chen and MacDonald 2006; McCabe et al. 2008; Horner-Devine et al. 2015).

Mixing in plumes and other stratified systems can be described in terms of a salt balance; assuming negligible horizontal mixing, the balance can be expressed as

$$\frac{D\overline{S}}{Dt} = \frac{\partial}{\partial z}\overline{S'w'}, \tag{1}$$

where S is salinity, the notation D/Dt indicates the material derivative, w is the vertical velocity, the overbar symbol indicates

Corresponding author: Samuel E. Kastner, sam.kastner@wwu.edu

DOI: 10.1175/JPO-D-21-0286.1

a Reynolds-averaged quantity, and the prime denotes a fluctuation. The material derivative of salinity represents the change in salinity a small parcel of water experiences as it moves through the plume, i.e., following a Lagrangian reference frame. The eddy diffusivity parameterizes the vertical turbulent salt flux (hereinafter referred to as simply vertical salt flux, dropping the "turbulent"), such that

$$\overline{S'w'} = -K_z \frac{\partial \overline{S}}{\partial z}, \tag{2}$$

where K_z is the eddy diffusivity of salt in the vertical direction (hereinafter referred to as simply eddy diffusivity, dropping the "of salt"). Eddy diffusivity values in river plumes typically vary from $O(10^{-4})$ to $O(10^{-2})$ m^2 s^{-1} (MacDonald and Geyer 2004; McCabe et al. 2008). Most river plume studies are primarily based on shipboard observations and Eulerian moorings, and so do not calculate $D\overline{S}/Dt$ (hereinafter referred to as the mixing rate or DS/Dt, dropping the overbar). Drifter based plume studies have utilized a control volume technique to calculate a vertical salt flux comparable to shipboard and mooring studies (McCabe et al. 2008; Kastner et al. 2018). River plume vertical salt fluxes are typically of order $O(10^{-2})$ psu m s^{-1} (MacDonald and Geyer 2004; McCabe et al. 2008; Kastner et al. 2018). Mixing can also be quantified by the spatial salinity variance, which represents the mean deviation of salinity in a system from the mean salinity of that system (MacCready et al. 2018). The destruction of spatial salinity variance is directly related to mixing.

b. River plumes in the surf zone

River water is often trapped in the surf zone at the Quinault River mouth and can be predicted based on the relationship between the surf zone width and the near-field plume length scale (Kastner et al. 2019). Once plume water is trapped in the surf zone, it is no longer forced by its initial momentum and is strongly influenced by surf-zone forcing (Wong et al. 2013; Olabarrieta et al. 2014; Rodriguez et al. 2018; Kastner et al. 2019; Jennings et al. 2020). In a saturated surf zone, waves break at a depth d proportional to their height H_s, such that $\gamma = H_s/d$ is constant throughout the surf zone. Wave height therefore decreases with depth approaching the shoreline, resulting in gradients in wave energy flux and radiation stress (momentum flux) that cause the surf zone to be turbulent and energetic.

Wave energy flux gradients in the surf zone are related to local energy loss rates (Battjes and Janssen 1978; Thornton and Guza 1983). The TKE dissipation rate ε is high in the surf zone, with typical values of $\varepsilon = O(\text{from } 10^{-4} \text{ to } 10^{-2})$ W kg^{-1} near the surface (Thornton and Guza 1983; George et al. 1994; Feddersen and Trowbridge 2005; Feddersen 2012a; Thomson 2012). For dissipative beaches, waves break consistently onshore of the break point, resulting in a flux of TKE through the water surface. The vertical structure of TKE dissipation rate has been found to scale with the wave height and water depth and inversely with distance from the water surface, such that dissipation is higher closer to the surface and closer to the break point (Longuet-Higgins and Stewart 1962; Thornton and Guza 1983; Feddersen 2012b).

Wave radiation stress gradients in the surf zone force alongshore currents with velocities on the order of v from 0.5 to 1.5 m s^{-1} (Longuet-Higgins and Stewart 1962; Thornton and Guza 1986; Spydell et al. 2007). In addition to mean currents, vertical vorticity introduced by short-crested breaking waves, wave groups, and shear instability cause the formation of energetic horizontal eddies (Peregrine 1998; Haller et al. 1999; Bowen and Holman 1989; Clark et al. 2012; Feddersen 2014). These eddies mix gradients in the cross- and alongshore directions, leading to large horizontal dispersion within the surf zone, with horizontal eddy diffusivity $K_x \approx O(\text{from 0.1 to 10})$ m^2 s^{-1} (Spydell and Feddersen 2009; Clark et al. 2010; Spydell and Feddersen 2012; Hally-Rosendahl et al. 2014). A variety of measurement techniques have been used to quantify surf-zone dispersion, including dye (Hally-Rosendahl et al. 2014) and drifting buoys (Spydell and Feddersen 2012). This high dispersion within the surf zone does not result in significant exchange with the neighboring inner shelf on short time scales (MacMahan et al. 2004; Hally-Rosendahl et al. 2014); however, rip currents can lead to significant exchange with the inner shelf, particularly on time scales of ~1 day (Reniers et al. 2009; Clark et al. 2012; Moulton et al. 2017; Kumar and Feddersen 2017a,b).

Several recent studies have shown that surface wave breaking outside the surf zone (whitecapping) can affect plume mixing in deeper water. Whitecapping is generally a less energetic forcing mechanism than surf-zone wave breaking and tends to produce lower TKE dissipation rates (Terray et al. 1996; Feddersen et al. 2007; Gerbi et al. 2009). Breaking waves can significantly contribute to river plume mixing when the plume layer is shallow and slow moving far from the river mouth (Gerbi et al. 2015), or when strong wave breaking is collocated with a plume front (Thomson et al. 2014). In particular, Gerbi et al. (2015) show that breaking waves are most effective at mixing a surface layer when the layer is thin, suggesting that the spatial dislocation of the generation of turbulence from a density gradient can impact mixing rates. Breaking waves can impact the structure of a river plume far from the river mouth where the plume propagates as a buoyant coastal current (Gerbi et al. 2013), but these effects are less important closer to the mouth where river momentum is large (Akan et al. 2017; Kastner et al. 2018).

Prior studies of small plumes in the surf zone have suggested the importance of breaking wave-driven mixing increasing plume entrainment velocity (Kastner et al. 2019) and injecting TKE at the surface that mixes the plume (Rodriguez et al. 2018). Because of the higher TKE dissipation rate in the surf zone (from 10^{-4} to 10^{-2} W kg^{-1}) relative to river plumes (from 10^{-8} to 10^{-3} W kg^{-1}), we expect wave-breaking processes to be the primary source of turbulence at the Quinault River mouth. However, a full analysis of wave-driven turbulence and stratification in shallow water has not been done, although some of the mechanisms discussed above for deeper water may be relevant.

In this study, we use novel in situ measurements to investigate the stratification and mixing of surf-zone-trapped river plume water that is exposed to wave-generated turbulence. The surf zone at the Quinault River mouth is shallow, wide, and saturated with energetic breaking waves, making it dangerous to conduct shipboard observations. For this reason our mixing estimates are based on measurements from drifters that follow

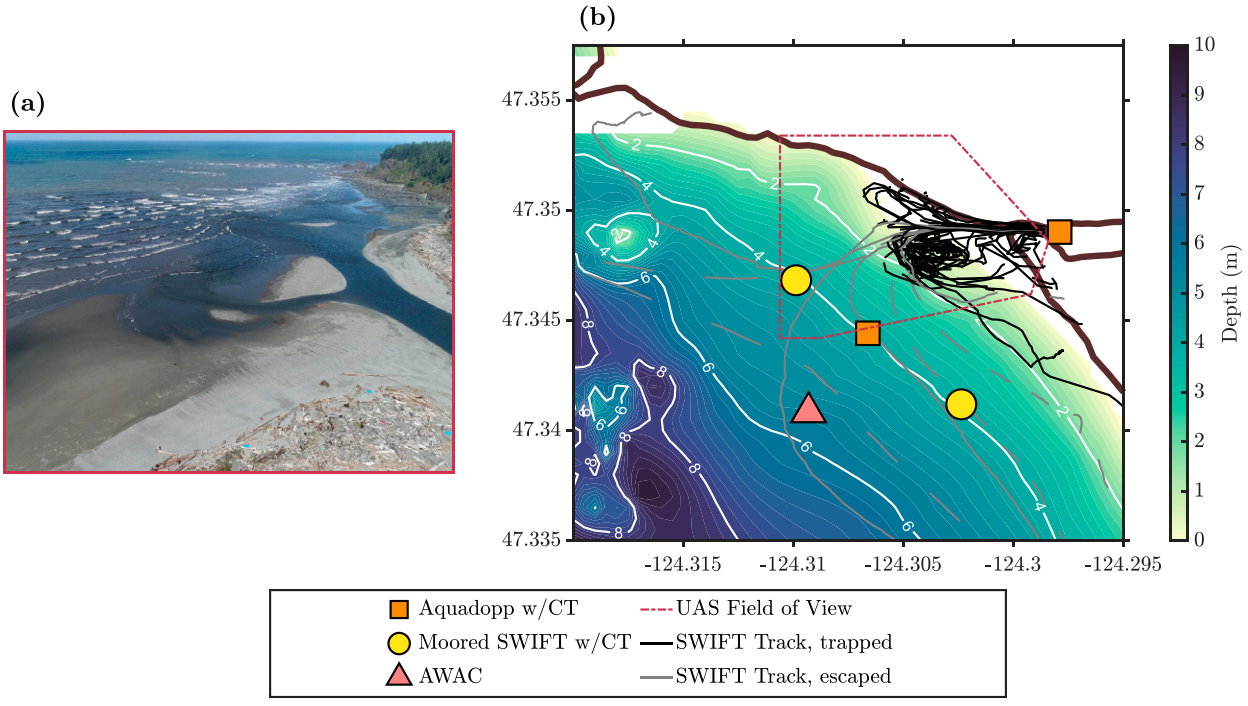

FIG. 1. The observational field campaign at the Quinault River mouth: (a) an example UAS perspective image from 28 Apr 2017, when the offshore wave height $H_s = 1.62$ m, the river volume flux $Q_T = 181$ m^3 s^{-1}, and the tidal stage is -0.41 m, and (b) a map of deployed instruments and bathymetry. Color shading indicates depth, and isobaths are given as white lines with notations in meters. Orange squares indicate moorings using Nortek Aquadopp ADCPs, yellow circles indicate moorings using SWIFTs, and the red triangle indicates the offshore AWAC. The UAS field of view is given as a dashed–dotted red line, and SWIFT drift tracks on 30 Apr 2017 are thin solid lines (black for trapped drifters and gray for escaped drifters). The shoreline is indicated with a thick solid brown line.

the trapped plume water and moorings at the edge of the surf zone. These measurements allow us to make calculations of stratification, the material derivative of salinity, vertical eddy diffusivity, and TKE dissipation rate (section 2). These quantities are related to each other and to tidal variability in river volume flux such that tidal variability leads to changes in mixing (section 3). Last, we discuss the implications of these findings on stratified turbulence in the surf zone, examine the potential impacts of lateral dispersion in the surf zone, and compare surf-zone-trapped river plumes with more conventional plume systems (section 4).

2. Methods

a. Observations

The data presented here were collected as part of an observational campaign described in detail by Kastner et al. (2019) at the Quinault River mouth, on Quinault Indian Nation land by Taholah, Washington (Fig. 1). The observations were made with the permission and guidance of the Quinault Nation Division of Natural Resources. We focus in this work primarily on measurements from the SWIFT (Surface Wave Instrument Float with Tracking) drifting buoys deployed in the river inlet. A table detailing the deployment time, model, tidal stage, and wave height for all SWIFT deployments that resulted in surf-zone-trapped drifters is shown in the appendix (Table A1). A map of drifter tracks subset by tidal stage is available in Kastner et al. (2019) (Fig. 3). Two models of SWIFTs were used, as detailed in Table 1. Figures 2 and 3 show examples of raw, high-resolution observations of salinity (Figs. 2b and 3b), drift speed (Figs. 2c and 3c), and heave (Figs. 2d and 3d), as well as estimates of TKE dissipation rate, stratification, and the material derivative of salinity (Figs. 2e and 3e) from two SWIFTv3s that were trapped in the surf zone on 30 April and 1 May 2017. The estimates of mixing rate and $\partial\overline{S}/\partial z$ (hereinafter referred to as stratification or $\partial S/\partial z$, dropping the overbar) shown in Figs. 2f, 2g, 3f, and 3g are calculated using the methods outlined in section 2b. We use the SWIFT measured raw heave to estimate significant wave height on 1-min intervals as $H = 4\sigma_z$, where σ_z is the standard deviation of the heave data over 1 min. This combination of measurements effectively resolves

TABLE 1. The instrumentation and specifications of the two versions of SWIFT drifters used during the Quinault observational campaign.

Model	Version 3	Version 4
Draft (m)	1.05	0.25
No. of CTs	3	1
CT depth (m)	0.1, 0.5, and 1.05	0.2
ADCP Model	Aquadopp HR (2 MHz)	Signature (1 MHz)

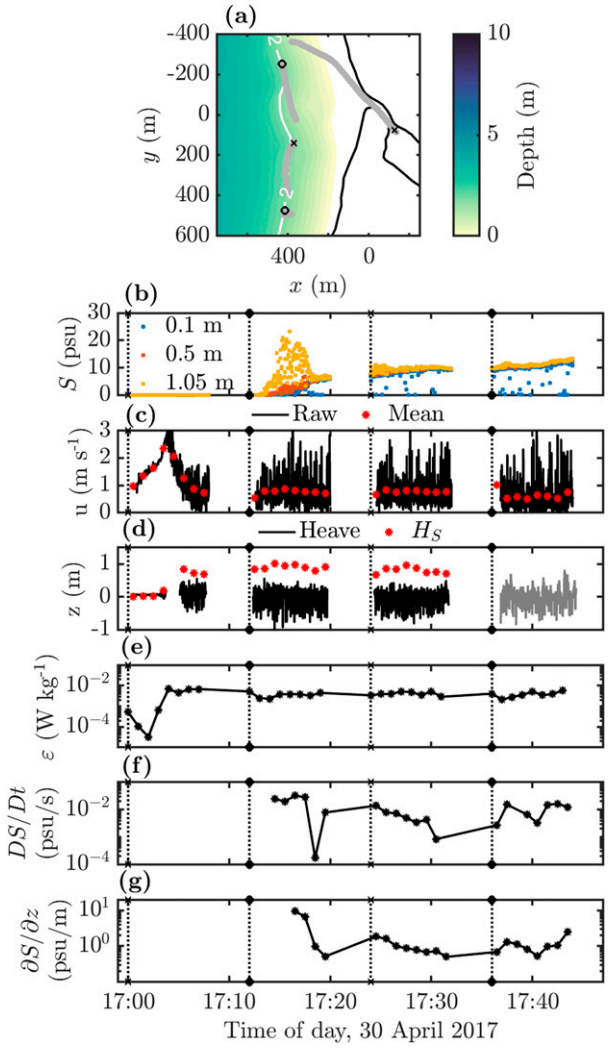

FIG. 2. Data from a SWIFTv3 deployed on 1 May 2017; this SWIFT was trapped in the surf zone: (a) the drift track overlaid on the bathymetry map from Fig. 1b transformed into a local coordinate system; (b) the 0.5-Hz salinity data at 0.1-, 0.5-, and 1.05-m depth; (c) the raw 4-Hz drift speed data from the GPS in black, with 1-min averages in red; (d) the raw 15-Hz inertial measurement unit heave data in black, with 1-min calculations of $H_S = 4\sigma_z$ in red (gray lines show data screened as poor quality by SWIFT data processing routines); (e) the vertical average over the top 0.5 m of structure function estimates of TKE dissipation rate from 1 min of uplooking Aquadopp HR ADCP data (Thomson 2012; Thomson et al. 2019); (f) the 1-min mixing rate DS/Dt at 0.5-m depth determined by the fitting method in section 2b; and (g) stratification $\partial S/\partial z$, also determined by the fitting method in section 2b. Alternating crosses and circles indicate the beginning of each SWIFT data collection burst.

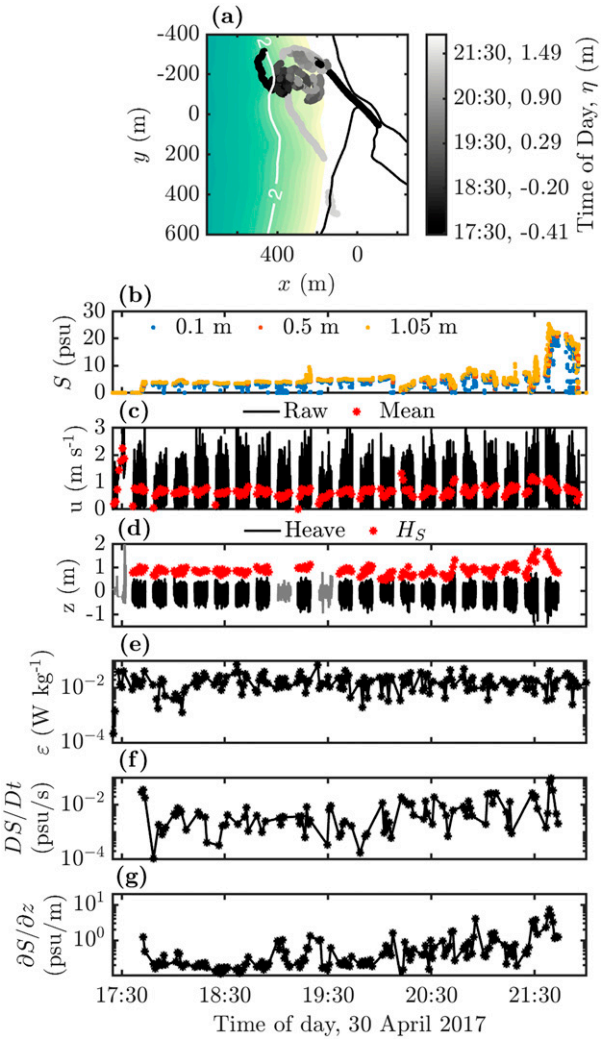

FIG. 3. Data from one SWIFTv3 and one SWIFTv4 deployed on 30 Apr 2017; both SWIFTs were trapped in the surf zone as the tidal stage rose from $\eta = -0.4$ m to $\eta = 1.7$ m as shown below the x-axis label (in all panels, data from only one SWIFT is shown for clarity; however, the two SWIFTS followed similar drift tracks and parameters matched well when data products overlapped): (a) the SWIFTv3 drift track overlaid on the bathymetry map from Fig. 1b transformed into a local coordinate system (the SWIFT track is colored by time, with black corresponding to times near deployment and light gray corresponding to times near recovery); (b) the 0.5-Hz salinity data at 0.1-, 0.5-, and 1.05-m depth from the SWIFTv3; (c) the raw 4-Hz drift speed data from the GPS on the SWIFTv3 in black, with 1-min averages in red; (d) the raw 15-Hz inertial measurement unit heave data in black, with 1-min calculations of $H_S = 4\sigma_z$ in red (gray lines shows data screened as poor quality by SWIFT data processing routines); (e) the vertical average over the top 0.5 m of structure function estimates of SWIFTv4 TKE dissipation rate from 1 min of downlooking Signature1000 HR ADCP data (Thomson 2012; Thomson et al. 2019); (f) the 1-min mixing rate DS/Dt at 0.5-m depth on the SWIFT v3 determined by the fitting method in section 2b; and (g) stratification $\partial S/\partial z$, also determined by the fitting method in section 2b.

wave-driven processes, plume dynamics, and mixing on time scales varying from seconds to the drifter's deployment length.

We use nearshore moorings with YSI Sonde 600LS CTD sensors ~1 and ~3 m below the water surface deployed at the surf-zone edge in ~4-m water depth (relative to mean lower

TABLE 2. Conditions over the course of the entire Quinault field campaign and on 30 Apr and 1 May 2017. Significant wave height H_s is calculated from the AWAC, River discharge Q_R is calculated as 150% of the Quinault Lake discharge per information from the Quinault Nation Division of Natural Resources, and tidal stage in meters above lower low water is taken from the USGS Point Grenville tide gauge.

	All observations			30 Apr 2017			1 May 2017
Quantity	Mean	Min	Max	Mean	Min	Max	At deployment
H_s (m)	1.64	1.00	2.3	1.81	1.51	2.05	1.4
Q_R ($m^3\ s^{-1}$)	156	114	217	139	139	140	132
Tidal stage (m)	1.31	−0.53	2.89	0.74	−0.40	1.98	0.02

low water at the USGS Point Grenville station) to measure the salinity field along the onshore edge of the inner shelf. At the boundaries of the surf-zone-plume system, we use measurements of spectral wave properties from a Nortek Acoustic Waves and Currents (AWAC) instrument deployed in ~6-m water depth as an offshore wave condition as well as a downlooking Nortek Aquadopp and bottom-mounted Onset HOBO pressure sensor deployed at the river mouth to capture the tidally varying river momentum and volume flux. The results presented in section 3 use data from the entire 2-week study period, focusing on two drifter deployments that occurred on 30 April and 1 May 2017. Mean, maximum, and minimum offshore wave height H_s, river discharge Q_R, and tidal stage for the whole study period and for the specific deployments examined in section 3a are shown in Table 2 (see also Kastner et al. 2019, their Fig. 2).

b. *Estimating mixing and stratification in the surf zone*

We use drifter measurements of salinity to quantify mixing as the material derivative of salinity, DS/Dt. This can be estimated from a single drifter and is therefore robust to the deployment constraints of the Quinault River mouth. Measurements from SWIFTs have been used in previous surf-zone studies (Zippel and Thomson 2015; Moghimi et al. 2016). Salinity measurements reported in this work are 1-min averages of the 0.5-Hz SWIFT CT data, except as noted.

The material derivative of salinity, DS/Dt, is calculated for each salinity sensor on a SWIFT drifter, either at three depths for the SWIFTv3 (0.1, 0.5, and 1.05 m) or at a single depth for the SWIFTv4 (0.2 m). We apply a third-order median filter to minimize the influence of bubbles, which cause spurious low salinity spikes in the raw data collected at 0.5 Hz, and obtain 1-min salinity averages. We calculate DS/Dt as the slope of a linear best fit to a 1-min time series of salinity data from each SWIFT CT sensor. We assume that an approximation of local linearity is reasonable over the 1-min period. The CT sensor resolution leads to uncertainty in DS/Dt of 1×10^{-5} psu s^{-1}. We exclude very fresh water, where $S < 0.5$ psu, from fits. This primarily occurs inside and near the river mouth at the beginning of drift tracks.

The SWIFT buoys are not perfectly Lagrangian tracers. This can be partially quantified by comparing the drift speeds of the two SWIFT versions, the larger 1.05-m-draft SWIFTv3 and the smaller 0.25-m-draft SWIFTv4. The v3 SWIFT is $\sim O(10^{-2})$ m s^{-1} slower than the smaller-draft v4 SWIFT; this slight discrepancy is similar to previous comparisons of the v3 SWIFT with high-frequency radar measurements of surface currents (Lund et al. 2018). Note that this comparison accounts for the difference in SWIFT draft but cannot account for non-Lagrangian bias in the SWIFTv4 measurements. Multiplying this velocity difference by the cross-shore salinity gradient, $\partial S/\partial x \sim O(10^{-2})$ psu m^{-1}, as observed by the nearshore moorings and drifters, and integrating over the SWIFTv3 draft of 1.05 m yields an overestimate of DS/Dt due to the difference in SWIFT draft of $O(10^{-4})$ psu s^{-1}. This analysis establishes a threshold of $DS/Dt = 1 \times 10^{-4}$ psu s^{-1}, below which DS/Dt estimates may be biased by the non-Lagrangian behavior of the drifters. We therefore exclude values below this threshold from our analysis, which eliminates approximately 1% of DS/Dt estimates.

We can similarly assess the role of vertical advection $[w_{adv}(\partial S/\partial z)]$ by calculating the vertical velocity associated with the surfacing of the 4-psu isohaline shown between Figs. 5a and 5c. This isohaline transits 2 m vertically in approximately 2 h, corresponding to a vertical advective velocity of $O(10^{-4})$ m s^{-1}. This velocity occurs when $\partial S/\partial z = 0.5$ psu m^{-1}, yielding a possible vertical advective contribution to the material derivative of $O(10^{-4})$ psu s^{-1}, the same as estimated from draft and thus not altering the cutoff value chosen for exclusion as outlined above. Moreover, the values of DS/Dt throughout this period from which this vertical advective contribution is estimated are higher than $O(10^{-4})$ psu s^{-1}, showing that vertical mixing contributes more significantly than advection to the temporal evolution of salinity.

Previous drifter-based studies of river plumes have shown that drifters tend to be trapped in river plume fronts, as surface-following floats are unable to follow the strong frontal downwelling velocities (McCabe et al. 2008; Kakoulaki et al. 2014; Zippel and Thomson 2017; Kastner et al. 2018). It is impossible to exclude the possibility that fronts are present in the near-field Quinault plume without transect data, which are not feasible for practical and safety reasons. However, we see little evidence of fronts in the surf zone from uncrewed aerial system (UAS) imagery and no evidence that drifters are trapped in front based on analysis of the drifter tracks at the Quinault River mouth (Figs. 1b, 2a, and 3a), or in the drifter behavior described in Kastner et al. (2019). Previous studies where drifters are trapped in river plume fronts show that the drifters trace out plume streamlines as they move away from the river mouth, spreading slightly away from each other; at any given time in these studies, all drifters are roughly the same radial distance from the river mouth, spaced out laterally along the river plume

front (McCabe et al. 2008; Kakoulaki et al. 2014; Kastner et al. 2018). We do not observe this drift track pattern in SWIFT deployments at the Quinault River mouth.

Using the SWIFTv3 measurements of salinity at three vertical positions, we calculate a local stratification $\partial S/\partial z$ as the slope of a linear fit to all three salinity measurements. This stratification will be used alongside DS/Dt in section 3c to calculate a vertical eddy diffusivity of salt. We estimate vertical eddy diffusivity, K_z, from the Lagrangian salt budget [Eqs. (1) and (2)]. Vertically integrating DS/Dt as estimated at each SWIFTv3 CT sensor using trapezoidal numerical integration and assuming that DS/Dt does not change between the CT measurement at 0.1 m and the surface yields an expression for near-surface vertical salt flux in terms of the vertical eddy diffusivity and the stratification in the top 1.05 m:

$$\int \frac{DS}{Dt}\, dz = K_z \frac{\partial S}{\partial z}. \tag{3}$$

We can therefore calculate K_z for each 1-min SWIFTv3 average calculation of DS/Dt and $\partial S/\partial z$. The results presented below are not sensitive to the averaging time scale as long as it is longer than a few wave periods (i.e., >25 s) and short enough for the stationarity of statistics [i.e., the length of a SWIFT data collection burst, <10 min; see Thomson (2012)].

To generate SWIFT TKE dissipation rate estimates we use a structure function method to estimate ε in the top 0.5 m of the water column (Thomson 2012; Thomson et al. 2019). Many of the raw Doppler velocity measurements are obscured by the high void fraction in the surf zone and so we apply a multiplicative correction factor of 3 to all dissipation rate estimates following Derakhti et al. (2020). Most SWIFT measurements do not resolve the wave energy flux gradient $\partial \mathbf{F}/\partial x$, because the drifters frequently transit as much or more alongshore than cross-shore once they enter the surf zone. Such SWIFT estimates of the cross-shore wave energy flux gradient are therefore contaminated by lateral variability driven by alongshore variability in bathymetry and noninfinite wave crest lengths due to directional spread (Dalrymple 1975). We therefore compare the dissipation rate estimates with a mean value for $\partial \mathbf{F}/\partial x$ over the course of the SWIFT deployment, where $\mathbf{F} = Ec_g$ is determined using the AWAC measurements of incident wave energy spectra E and the group velocity c_g. After applying the void correction factor, depth-averaged values of SWIFT-estimated TKE dissipation rate in the top 0.5 m agree well with depth-averaged bulk estimates of surf-zone dissipation based on the wave energy flux gradient $(1/d)\partial \mathbf{F}/\partial x$, where d is the water depth (not shown).

For drifts that recirculate (Fig. 3), we are able to assess the agreement between dissipation estimates from the SWIFT HR ADCPs and a calculation of $(1/d)\partial \mathbf{F}/\partial x$ from SWIFT measured wave properties and position. The SWIFT dissipation estimates in the top 0.5 m are roughly one-third as large as $(1/d)\partial \mathbf{F}/\partial x$, showing reasonable agreement in the limited data available. The bottom CT sensor of the SWIFTv3 is at 1.05-m depth; only about 4% of our measurements occur in the bottom 20% of the water column, where the role of the bottom boundary layer is expected to be important (Feddersen and Trowbridge 2005). We therefore assume that our turbulence measurements are due to surface injection from breaking waves, and we do not examine the role of surf-zone bottom boundary turbulence in mixing the Quinault River plume.

The beach near the Quinault River mouth is dissipative during moderate to high wave forcing conditions, when river water to be trapped in the surf zone. Depth decreases monotonically onshore of the 4-m isobath; therefore, the beach is always dissipative at low water (Fig. 5). Wave breaking does not always occur in the deeper river channel; however, such breaking is required for river water to be trapped in the surf zone, especially at high water (Kastner et al. 2019). Therefore, the beach near the Quinault River mouth is dissipative when river water is trapped in the surf zone, the focus of this study.

We define $\overline{S_t'^2}$ as the mean of the squared differences of the median filtered salinity value from the fitted salinity value such that

$$\overline{S_t'^2} = \frac{1}{f_s T_{\text{win}}} \sum [S_{\text{fit}}(t) - S(t)]^2, \tag{4}$$

where $f_s = 0.5$ Hz is the CT sampling frequency, $T_{\text{win}} = 60$ s is the averaging window, the sigma operator indicates a summation over T_{win}, $S(t)$ is the median filtered salinity at a time t within the window, and $S_{\text{fit}}(t)$ is the linear salinity fit found in order to calculate DS/Dt, evaluated at the same time t. Propagating error from the SWIFT's onboard Aanderaa 4319 CT sensor indicates that the error associated with this calculation is ~1% of the calculated value. The mean square salinity error as defined above represents the scatter around the linear fit DS/Dt. In these calculations, we assume that our 1-min averaging window and salinity thresholds are sufficient to achieve local linearity. In this case, $\overline{S_t'^2}$ only represents the scatter around the best fit line. If instrument noise and non-Lagrangian bias are small, then the local turbulent fluctuations dominate $\overline{S_t'^2}$, and we expect $\overline{S_t'^2}$ to be related to DS/Dt, as shown in Fig. 4b. The strong relationship between DS/Dt and $\overline{S_t'^2}$ indicates that DS/Dt is a good estimate of Quinault River plume mixing and is not significantly influenced by changes in salinity driven by plume spreading and shoaling of the plume interface (McCabe et al. 2008; Kastner et al. 2018). We will therefore use DS/Dt as an estimate of mixing throughout this paper.

The mean square salinity error [Eq. (4)] is similar to the spatial salinity variance introduced by MacCready et al. (2018) in that it is a squared salinity deviation, but differs in two key ways. First, the salinity variance is calculated using deviations from the spatial salinity mean, whereas $\overline{S_t'^2}$ is calculated using residuals from a fit line. Second, intense mixing is indicated by high $\overline{S_t'^2}$, whereas a sharp decrease in spatial salinity variance indicates intense mixing.

3. Results

a. The structure of a surf-zone-trapped river plume

We show data from two example SWIFT deployments in Figs. 2 and 3, which took place during wave, river discharge,

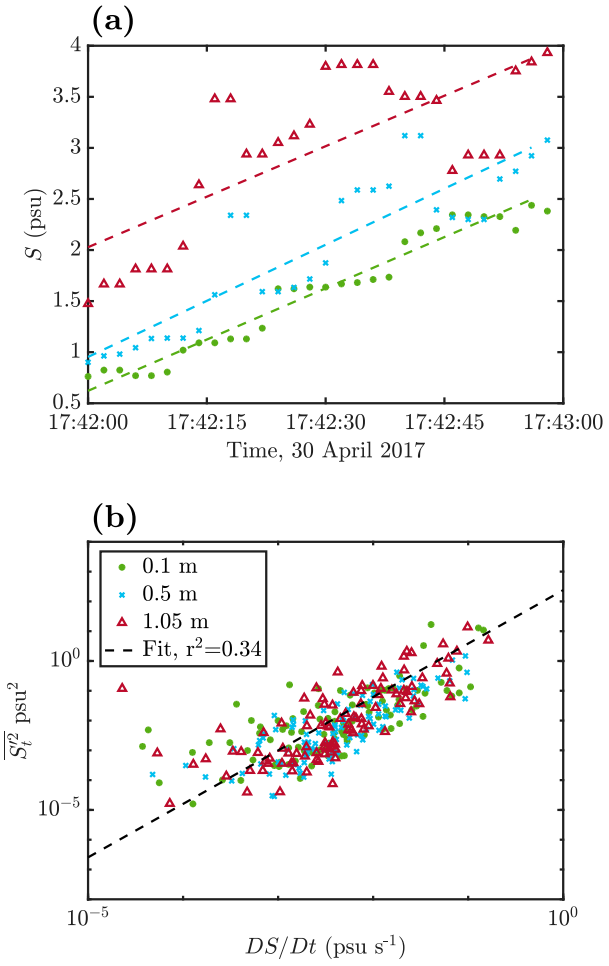

FIG. 4. Estimates of DS/Dt and $\overline{S_t'^2}$ using salinity observations from a SWIFTv3 deployed on 30 Apr 2017: (a) median filtered salinity data and the linear fits used to calculate DS/Dt at each CT sensor depth, as indicated by symbols (all $r^2 > 0.99$), and (b) the comparison of $\overline{S_t'^2}$ and DS/Dt for each CT sensor depth (indicated by symbols) for all SWIFTv3 1-min averages on 30 Apr 2017.

and tidal conditions that were close to average for the 2-week observational period (Table 2). On 1 May 2017, one SWIFTv3 traveled 1750 m through the surf zone over 48 min before beaching south of the river mouth. It reached a maximum speed of 2.35 m s^{-1} and experienced a maximum wave height of 1 m. Average near-surface TKE dissipation rate estimates ε were of order $\sim 2 \times 10^{-3}$ W kg^{-1}, and the onboard CT sensors measured a maximum salinity value of 23.3 psu at 1.05 m, concurrent with a salinity of 0.7 psu at 0.1 m (Fig. 2). As the drifter transited through the surf zone, the measured salinity increased continuously, the measured significant wave height and the estimated TKE dissipation rate increased before leveling off, and the drift speed peaked near the river mouth before decreasing to a near-constant value of ~0.75 m s^{-1}.

On 30 April 2017, one SWIFTv3 and one SWIFTv4 were deployed concurrently in the river mouth. The drifters were deployed at low water and recirculated in a region within ~500 m south of the river mouth for a period of 5 h before beaching (until almost high water; Fig. 3a). A similar event occurred on 5 May 2017, but the SWIFTs deployed on that day did not have functioning CT sensors after several beaching events. Both of these events occurred during normal wave conditions for our deployment period and at different river discharges (Table 2), suggesting that this recirculation may be a common feature of the surf-zone circulation at the Quinault River mouth. The 30-min-average cross-shore position (normalized with respect to the surf-zone width) of the SWIFTs deployed on 30 April 2017 did not change with tidal stage. SWIFTv3 measurements from 30 April 2017 show that surf-zone salinity increases sharply at first as the drifter enters the surf zone, slowly over the next ~3 h as it recirculated within the surf zone, and then sharply again at the end of the deployment as it exited the recirculation zone, transited southward, and beached (Fig. 3b). Heave (from the SWIFTv3) and TKE dissipation measurements (from the SWIFTv4) showed a similar pattern to the deployment on 1 May 2017, increasing as the drifter exited the river mouth and entered the surf zone before leveling off in magnitude. TKE dissipation rate is approximately constant in the surf zone, with $\varepsilon \approx 10^{-2}$, consistent with previous studies (Figs. 3d,e).

The deployments on 30 April and 1 May 2017 show similar patterns of evolution in 0.5 m depth mixing rate and stratification in their initial 40 min of deployment (Figs. 2f,g and 3f,g). As the drifters leave the river mouth, enter the surf zone, and salinity begins to increase, the mixing rate drops from $DS/Dt > 10^{-2}$ psu s^{-1} near the river mouth to under 10^{-2} psu s^{-1}. During the longer deployment on 30 April 2017, the mixing rate increases as the drifters recirculate in the surf zone over 5 h; by the end of the deployment, DS/Dt was larger than its local maximum near the river mouth. Stratification also falls for both deployments during the first 40 min, in both cases by roughly one order of magnitude. Stratification is higher during the 40-min deployment on 1 May than during the initial 40 min of the deployment on 30 April, but increases during the 30 April deployment and reaches values similar to those estimated on 1 May (~10^{-1} psu m^{-1}) by the end of the drift track. These increases in mixing rate and stratification on 30 April 2017 occur as tidal stage increased from low water at the beginning of the deployment to high water at the end of the deployment; higher mixing rates and stratification occur at higher tidal stage.

At the Quinault, total volume flux from the river mouth is maximum at low water, and minimum at high water due to volume storage within the estuary during flood tides. We define this volume flux as

$$Q_T = u_T d_T b_T, \tag{5}$$

where u_T is the depth-averaged velocity at the river mouth (including both river and tidally driven components), d_T is the tidally varying river mouth depth, and the effective river mouth width $b_T \approx 87$ m is defined as in Kastner et al. (2019). A time series of u_T can be found in Kastner et al. (2019), Fig. 2, and values of Q_T during the example drifts shown in Figs. 2 and 3 are shown in Table 2. The discharge at the river mouth is always completely fresh; thus, total freshwater

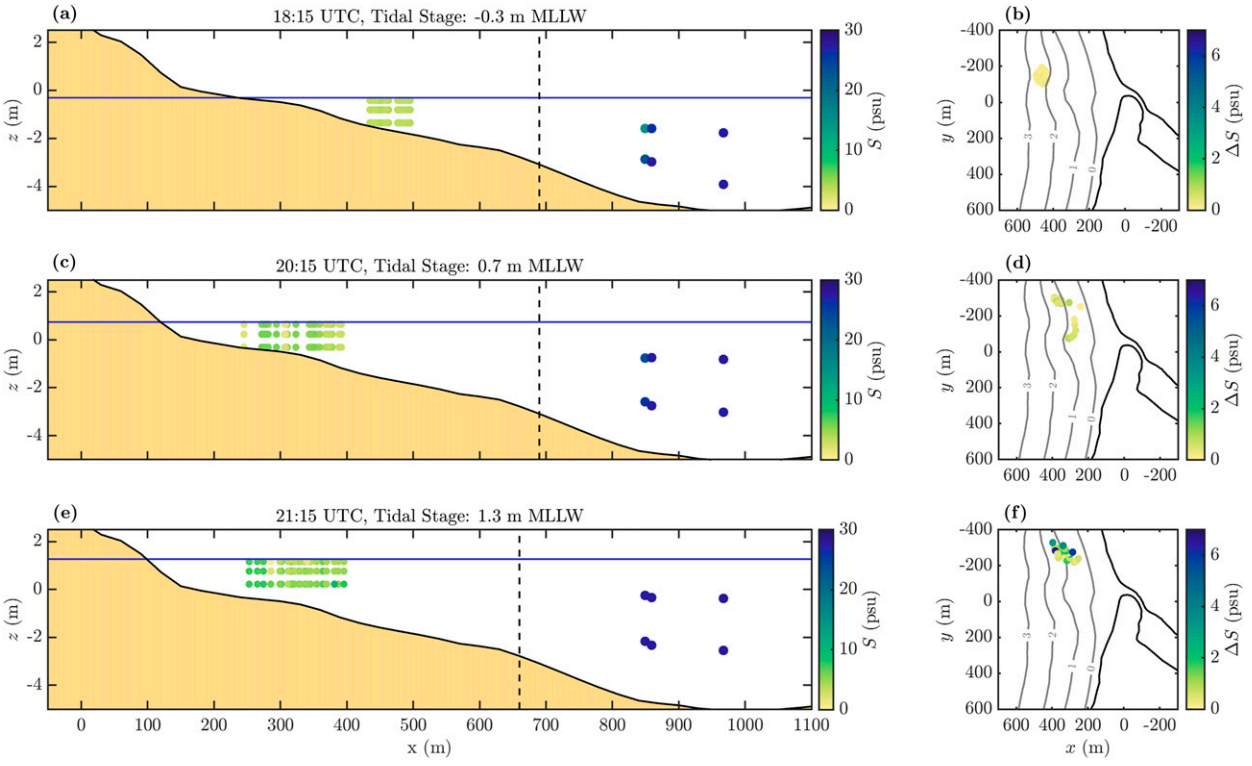

FIG. 5. (a),(c),(e) Color scatterplots showing the salinity structure across the surf zone to the inner shelf as measured by the SWIFTv3 and the moorings on 30 Apr 2017 alongside (b),(d),(f) maps showing the location of the drifter measurements shown in the corresponding cross section, colored by the salinity difference between the 1.05- and 0.1-m CT sensors. Time advances, and tidal stage increases, from (a) and (b) to (e) and (f). The solid black line and tan-filled region in (a), (c), and (e) indicate the seabed (note that depth changes as the tidal stage increases), and the vertical dashed black line indicates the surf-zone width, calculated using linear wave energy flux conservation as described in Kastner et al. (2019). The breaker depth increases as the offshore significant wave height increases during the deployment from close to the minimum to close to the maximum values for 30 Apr 2017 (Table 2); this surf-zone widening is also visible in the UAS imagery (not shown). The colored dots inside the surf zone in (a), (c), and (e) indicate all 1-min salinity averages from the SWIFTv3 in the 30-min window centered on the time indicated in the panel title, and the colored dots outside the surf zone indicate the average salinity measured by the moorings within the 30-min window. The mooring data points are shown larger to emphasize that they are 30-min-average salinity values, as opposed to the 1-min-averaged SWIFT data. In (b), (d), and (f), the solid black line indicates the coastline, as in Fig. 1b, and the gray contours indicate bathymetry, with values in meters relative to mean lower low water.

discharge is also tidally modulated, with a minimum at high water and a maximum at low water. The surf zone is also widest and extends farthest offshore at low water (given a constant wave condition) due to the concave beach shape (Kastner et al. 2019). Salinity measurements from 30 April 2017 show that minimum salinity occurs at low water, when the drifters are deployed, and increases with the tidal stage (Figs. 3b and 5). Salinity at the inner shelf moorings also increases with tidal stage during this time period, particularly at the south mooring (Fig. 5). Simultaneously, the mooring salinity difference between 1 and 3 m decreases with tidal stage (Fig. 5). Water at the moorings is always saltier than in the surf zone. Thus, from low to high water on 30 April 2017, the surf zone makes a transition from fresh and unstratified to saltier and stratified. As mixing rate estimates increase with tidal stage coincident with increased stratification, we might expect that variability in vertical eddy diffusivity would be small, or even that vertical eddy diffusivity would be constant [Eqs. (1) and (2)]. This relationship will be examined in section 3c.

TKE dissipation rate estimates from the SWIFTv4 do not show any dependence of ε over the course of the deployment (Fig. 3e). Together with the changes in DS/Dt observed in Fig. 3f the lack of dependence on ε suggests that DS/Dt increases irrespective of ε; in other words, increases in mixing are not driven by increases in turbulence and instead correspond to an increase in $\partial S/\partial z$. This differs from many river plume studies, which have shown that more intense mixing generally occurs in regions with higher TKE dissipation rate (McCabe et al. 2008; Jurisa et al. 2016; Geyer et al. 2017). We attribute the increase in $\partial S/\partial z$ to tidal modulation of the riverine freshwater flux in section 4a. Additionally, we do not see evidence of an increase in TKE dissipation rate with offshore wave height (not shown), indicating that the surf zone at the Quinault River mouth may be saturated by

breaking waves. In a saturated surf zone, TKE dissipation rate at any cross-shore location is primarily a function of bathymetry, as depth-limited breaking occurs from the break point to the shoreline on a dissipative beach (Wright et al. 1982; Raubenheimer et al. 1996).

Figure 6 shows the ensemble average of S, u, H, ε, DS/Dt, and $\partial S/\partial z$ along a drifter track in 450-m bins over the first 2 km of along-track distance. Salinity is normalized by the mean measured salinity at the nearshore moorings at the time of drifter deployment (or the time-averaged nearshore mooring salinity for drifter deployments when the moorings were not in the water), drift speed is normalized by the near-mouth maximum drift speed, and significant wave height is normalized by the wave height at breaking. These dimensionless quantities follow similar patterns to the along-track examples shown in Figs. 2 and 3 as a drifter leaves the river mouth: salinity increases before leveling off, wave height increases and levels off, and drift speed peaks early in the drift track before decreasing to a near-constant value. TKE dissipation rate increases slightly at the beginning of the drift track before leveling off, while mixing rate decreases continuously along an average drift track and stratification decreases quickly after an initial increase. These initial increases in salinity, wave height, TKE dissipation rate, and stratification, and peak in drift speed are associated with the drifter exiting the river mouth and entering the surf zone. The initial increase in stratification (Fig. 6f) is likely associated with shoaling of the plume interface after liftoff (MacDonald and Geyer 2004).

The along-track evolution of plume structure shown by the ensemble averages in Fig. 6 contrasts drifter observations of plume structure in the Columbia and Fraser River plumes outlined in McCabe et al. (2008) and Kastner et al. (2018), respectively. These plumes (and drift tracks) have a much larger spatial footprint than the Quinault River plume, with drift tracks extending for 10–15 km at the Fraser and ~35 km at the Columbia, but also have a larger discharge ($Q_R \sim 950$ m^3 s^{-1}for Fraser, and $Q_R \sim 7000$ m^3 s^{-1} for Columbia) and do not encounter surf-zone wave breaking. In both cases drifters were deployed seaward of plume liftoff; salinity tends to increase sharply at the beginning of the drift tracks before leveling off farther away from the river mouth, while velocity tends to behave inversely, decreasing sharply at the beginning of the drift tracks before leveling off.

Estimates of salt flux and stratification also differ from the Quinault versus the Columbia and Fraser river plumes. Vertical salt fluxes, calculated using a control volume method in both McCabe et al. (2008) and Kastner et al. (2018), are higher near the river mouth and decrease farther afield. A similar pattern is seen in stratification; these behaviors are analogous to the behavior of the mixing rates shown in Figs. 2, 3e, and 6e. McCabe et al. (2008) use Eq. (2) to calculate eddy diffusivity, finding that the decrease in vertical salt flux along a drift track outpaces the decrease in stratification, resulting in a decline in eddy diffusivity. TKE dissipation rate estimates from the Columbia River plume also decline offshore due to stratification suppressing

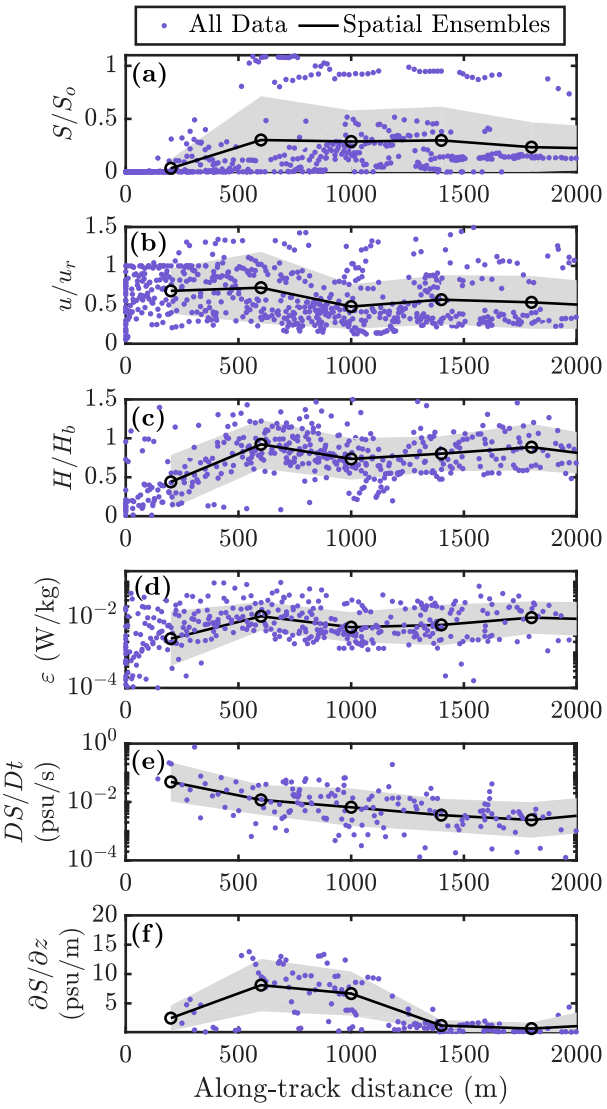

FIG. 6. Along-track plots of observed and estimated quantities from SWIFT drifters that were trapped in the surf zone: (a) salinity, normalized by the mean measured salinity at the nearshore moorings at the time of drifter deployment (or the averaged nearshore mooring salinity over the entire study period for drifter deployments when the moorings were not in the water); (b) drift speed, normalized by the maximum drift speed reached near the river mouth; (c) significant wave height, normalized by the height at breaking; (d) vertical averages in the top 0.5 m of structure function estimates of TKE dissipation rate estimates using SWIFT ADCP HR measurements; (e) the material derivative of salinity, estimated as detailed in section 2b; and (f) the stratification in the top 1.05 m from SWIFTv3s. Measurements from all SWIFTs are shown in (a)–(e); only measurements from SWIFTv3s are shown in (f). Blue points show 1-min-average quantities, and black open circles show ensemble averages of all observations and estimates of trapped SWIFTs in 400-m bins, as described in section 3a. The gray-shaded region shows 1 standard deviation away from the mean in the same bins.

turbulence (Kilcher et al. 2012; Jurisa et al. 2016), unlike the estimates presented in Figs. 2, 3d, and 6d, which show no trend in along-track distance. This lack of trend is likely due to the fact that the breaking wave generated turbulence in the surf zone is not related to the river volume flux, which controls stratification. This is a significant difference from larger plumes such as the Columbia where the two are linked and the combined tidal and river discharge is the primary source of turbulence and buoyancy (Horner-Devine et al. 2015; Jurisa et al. 2016).

Care must be taken in interpreting the along-track TKE dissipation rate, as we would expect a cross-shore gradient of TKE dissipation rate in the surf zone, with stronger dissipation toward the break point. The drifters mostly transit alongshore during any given deployment (Figs. 1b and 2), and so the ensemble-averaged TKE dissipation rate shown in Fig. 6d does not explicitly include cross-shore variability. The recirculating drifts shown in Figs. 3 and 5 allow us an opportunity to assess the impact of this cross-shore variability in TKE dissipation rate on DS/Dt; we do not observe a significant dependence of mixing rate on TKE dissipation rate (time series of each quantity shown in Fig. 3, direct dependence not shown). While we cannot rule out a dependence of mixing rate on TKE dissipation rate more generally, we find it more likely that stratification is instead a limiting factor on mixing, as described in more detail in sections 3c and 4c.

b. Cross-shore structure

High wave forcing (offshore H_S up to 2.3 m; Table 2) at the Quinault River mouth results in river water being mostly trapped in the surf zone during our observational period (Kastner et al. 2019). Salinity measurements from all surf-zone-trapped SWIFT drifters over the course of the entire study period show that the surf zone often remain fresh ($S < 10$ psu; 83% of measurements), whereas salinity measurements from the moorings just outside of the surf zone are significantly higher ($S > 25$ psu; 91% of measurements) (Fig. 7a). At ~1-m depth, the surf-zone SWIFTv3 salinity measurements are frequently more than 10 psu fresher than the inner shelf mooring measurements. Salinity does not vary significantly in the cross-shore direction within the surf zone, resulting in a large horizontal cross-shore salinity change near the surf-zone edge when the surf-zone salinity is low (Fig. 7). Although we observe a large salinity difference between the surf zone and inner shelf, there is no evidence of trapping in the drifter tracks as described in section 2b. We conclude that the intensity of mixing in this system prohibits the generation of a strong, convergent front.

Calculations of stratification (section 2b) indicate that the surf zone can be stratified (Fig. 7b). Specifically, the stratification in the upper 1.05 m of the surf zone is slightly higher on average (mean ~ 1.8 psu m^{-1}) than the offshore stratification between 1 and 3 m (mean ~ 0.72 psu m^{-1}). This differs from surf-zone studies conducted far from river mouths, which have shown the surf zone to be unstratified (e.g., Hally-Rosendahl and Feddersen 2016). Our results show that this is not necessarily true; in the vicinity of a moderate river discharge the surf zone can sustain levels of stratification similar to those

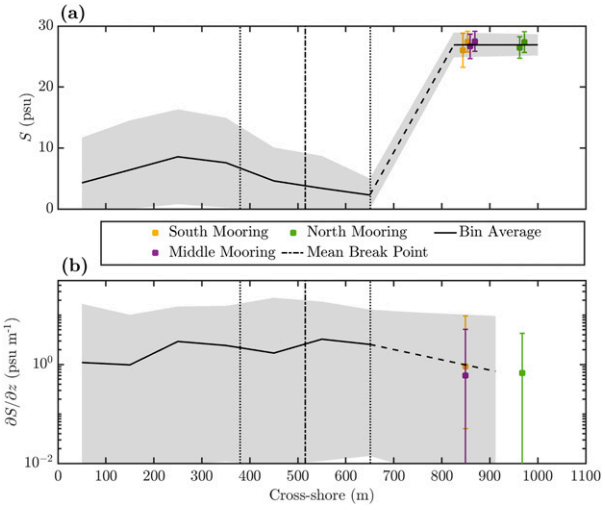

FIG. 7. Cross-shore profiles of quantities measured from trapped SWIFT drifters and nearshore moorings at alongshore positions less than 1500 m from the river mouth: (a) Cross-shore bin average of salinity with a bin size of 100 m; the shaded area represents the standard deviation of salinity in each bin. The deployment-average salinity for the nearshore moorings is also shown, with error bars indicating standard deviation. Salinity measurements from all surf-zone-trapped SWIFT drifters within the alongshore spatial constraint detailed above are included (see Table 1 for measurement depths). There are two points for each mooring, offset in the horizontal for clarity; the fresher point for each mooring is the 1-m CTD, and the saltier point is the 3-m CTD. (b) Cross-shore bin average of stratification with a bin size of 100 m; the shaded area represents the range of stratification in each bin, as well as the deployment-average salinity for the nearshore moorings, along with the mean and range of mid-water-column stratification from the moorings. The mean surf-zone width is given by the black dashed vertical line, with the black dotted lines indicating 1 standard deviation from the mean break point.

observed in larger plumes. For example, Fig. 6 from Kastner et al. (2018) provides values of near-surface stratification from the Fraser: ~10 psu m^{-1} at the liftoff peak and ~3 psu m^{-1} in the near-field plume. Thus, the Quinault stratification values of ~2 psu m^{-1} are similar in magnitude to the values observed in the near-field Fraser plume. We do not observe any significant cross-shore trend in surf-zone stratification (Fig. 7b). Note that the center of mass of the drifter locations remains roughly in the middle of the surf zone ($\overline{x}/L_{sz} = 0.67$, 0.48, and 0.5 for the times shown in Fig. 5), confirming that the observed changes in stratification are not the result of drifters sampling the edges of the surf zone where other processes may influence stratification.

c. Turbulence and mixing in the surf zone

We consider two surf-zone-mixing models based on Eq. (3); the simpler version assumes a constant value of vertical eddy diffusivity, K_z. To assess the validity of this simple model, we calculate an average value of the vertical eddy diffusivity based on all the available mixing rate and stratification

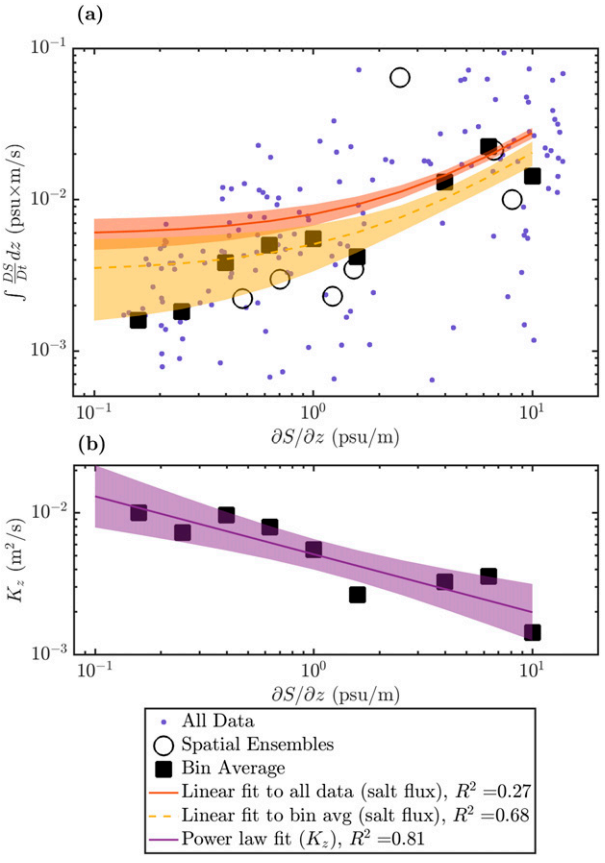

FIG. 8. We calculate a single, representative eddy diffusivity for the entire study period and show that eddy diffusivity can vary with stratification: (a) A demonstration of how eddy diffusivity can be estimated by the relationship between vertically integrated Lagrangian mixing rate on the y axis and the stratification on the x axis. SWIFTv3 data are shown as blue data points, and bin averages of vertical salt flux in stratification bins are shown as black squares. Ensemble-averaged values from Fig. 6 (i.e., binned in distance offshore) are shown as open black circles. Linear fits with a 68% confidence interval are shown with lines and a shaded area to represent the confidence interval. The solid red line indicates a fit to all estimates shown on this figure (blue dots); the dashed gold line indicates a fit to the bin averages (black squares). The slopes of these linear fits are estimates of the eddy diffusivity; the y intercept of the fits is representative of background mixing processes (Table 3). (b) The eddy diffusivity obtained by simply dividing the vertical salt flux and stratification values of the bin averages (black squares) in (a); the decreasing trend of this eddy diffusivity estimate with increasing vertical salt flux is well described by a log-linear power-law relationship of the form $K_z = a(\partial S^b/\partial z)$, where $a = 0.005$ and $b = -0.4 \pm 0.18$ m^3 psu^{-1} s^{-1} (fitting is done in log space; 95% confidence interval of a: $0.004 < a < 0.0065$).

measurements. We first bin average the vertically integrated mixing rate in logarithmic space stratification bins of width 0.2 (i.e., bin edges of 10^{-1}, $10^{-0.8}$ psu m^{-1}, etc.). The 1-min mixing rate and stratification products shown in Fig. 8a are significantly scattered from the bin averages. Allowing for a nonzero y intercept in the fit of vertically integrated mixing rate to stratification, Eq. (3) becomes

$$\int \frac{DS}{Dt} dz = K_z \frac{\partial S}{\partial z} + \mathscr{C}, \tag{6}$$

where $\mathscr{C}$ represents background mixing (perhaps due to lateral processes) as a constant value. We fit the relationship between stratification and vertically integrated mixing rate in four main ways: first, using all 1-min SWIFT estimates shown in Fig. 8a and allowing a nonzero y intercept as show in Eq. (6) (red line in Fig. 8, method I in Table 3), second, using the bin-averaged vertically integrated mixing rate and stratification and allowing a nonzero y intercept as show in Eq. (6) (gold line on Fig. 8a; method II in Table 3), third, using all 1-min SWIFT estimates shown in Fig. 8a and forcing a y intercept of zero as show in Eq. (3) (not shown in Fig. 8a; method III in Table 3), and finally using the bin-averaged vertically integrated mixing rate and stratification and forcing a y intercept of zero as show in Eq. (6) (not shown in Fig. 8a; method IV in Table 3). For fits to bin averages, we do not fit bins that contain less than 5% of all data. We tested to see whether the scatter in the data about these fits is dependent on wave, river, or tidal forcing but found no strong relationship for any of these forcing parameters (not shown).

Fitting all data shown in Fig. 8a yields a vertical eddy diffusivity $K_z = (2.1 \pm 0.55) \times 10^{-3}$ m^2 s^{-1} ($p < 1 \times 10^{-4}$), with $\mathscr{C} = (5.8 \pm 2.8) \times 10^{-3}$ psu m s^{-1} ($p < 1 \times 10^{-4}$) (Fig. 8a; method I on Table 3). The analysis results in a modest correlation ($R^2 = 0.27$; Fig. 8a) but yields a statistically significant linear fit and supports the conclusion that near-surface vertical mixing in the surf zone can be reasonably parameterized by a constant eddy diffusivity (statistics calculated in linear space). The data presented in Fig. 8a are heteroscedastic in linear space because the variance of salt flux increases as stratification increases. Therefore, the p values reported above and in Table 3 are calculated using the robust standard error method, which does not require data to be homoscedastic (White 1980). Note that in Fig. 8 error bars indicate 1 standard deviation from the mean to facilitate log-scale plotting; the uncertainty intervals in the text above, Table 3, and the figure caption are 95% confidence intervals obtained from fitting. Fitting the bin averages (method II on Table 3) yields similar values of K_Z and $\mathscr{C}$ as described above from method I. While this method is less statistically significant than method I because of the reduced sample size, we will use the bin-average calculations of vertically integrated mixing rate and stratification in section 4a and so include these fitting parameters for completeness. Using Eq. (3) to fit all the data shown in Fig. 8a (i.e., forcing the y intercept through zero; methods III and IV in Table 3), yields a slightly higher eddy diffusivity than found using Eq. (6) by methods I and II. This could be due to mixing caused by lateral processes being erroneously included as vertical mixing (e.g., Hally-Rosendahl et al. 2014; see section 4a). We do not observe strong trends in the residual of the fit calculated using Eq. (6) with either cross-shore or alongshore position (not shown).

TABLE 3. Eddy diffusivity and background mixing linear fitting parameters from different fitting methods, as specified in section 3c. Method I fits all 1-min SWIFT estimates of vertically integrated mixing rate and stratification using Eq. (6); method II fits bin averages of these same quantities using Eq. (6); method III fits all estimates of these quantities using Eq. (3), which has a y intercept of zero; method IV fits the bin averages using Eq. (3), which has a y intercept of zero. The p values shown in this table in parentheses are calculated using the robust standard error method, which does not require data to be homoscedastic (White 1980).

Fitting method	K_Z (m^2 s^{-1}) (p)	C (psu m s^{-1}) (p)	R^2
I (all data)	$(2.2 \pm 0.6) \times 10^{-3}$ ($p < 1 \times 10^{-4}$)	$5.8 \pm 2.8 \times 10^{-3}$ ($p < 1 \times 10^{-4}$)	0.27
II (bin average)	$(1.7 \pm 1) \times 10^{-3}$ ($p = 0.0211$)	$3.4 \pm 4.4 \times 10^{-3}$ ($p = 0.11$)	0.64
III (all data, zero y intercept)	$(2.8 \pm 0.5) \times 10^{-3}$ ($p < 1 \times 10^{-4}$)	0 (—)	0.20
IV (bin average, zero y intercept)	$2.2 \pm 0.9 \times 10^{-3}$ ($p = 6.2 \times 10^{-3}$)	0 (—)	0.53

The range of stratification for the study spans from $O(10^{-1})$ to $O(10^{1})$ psu m^{-1}, while the binned near-surface vertical salt flux spans a smaller range from $O(10^{-3})$ to $O(10^{-2})$ psu m s^{-1}. We therefore investigate whether the large range in stratification results in different values of eddy diffusivity. We take the vertically integrated mixing rate to be equal to the vertical salt flux (as described in section 2b) and calculate a variable eddy diffusivity by dividing bin averages of this vertically integrated mixing rate by stratification, yielding a range of $1.4 \times 10^{-3} < K_z < 1 \times 10^{-2}$ m^2 s^{-1}. The bin-averaged eddy diffusivity displays a strong dependence on stratification; eddy diffusivity is highest where stratification is low (Fig. 8b). A power law fit (linear in logarithmic space) represents the decrease in eddy diffusivity with increasing stratification well ($r^2 = 0.78$; $p = 1 \times 10^{-3}$). This fit takes the form $K_z = a(\partial S^b/\partial z)$, where $a = 0.005$ and $b = -0.4 \pm 0.18$ m^3 psu^{-1} s^{-1} (fitting done in log space; 95% confidence interval of a: $0.004 < a < 0.0065$). We note that there is autocorrelation in this fit, as $K_z \sim a(\partial S^{-1}/\partial z)$; however, the 95% confidence interval of the exponent b does not include -1, so the result presented above is robust to the autocorrelation.

The higher correlation and significance of the relationship between binned stratification and eddy diffusivity than the relationship between binned stratification and salt flux from Eq. (6) (gold line in Fig. 8a; method II in Table 3), which has the same number of fitting parameters, suggests that there may be limits on the effectiveness of a constant eddy diffusivity to model mixing in this system. Vertical mixing of a river plume in the surf zone may therefore be described by both a constant eddy diffusivity $K_Z \approx 2 \times 10^{-3}$ m^2 s^{-1} and a stratification-dependent eddy diffusivity, $1.4 \times 10^{-3} < K_z < 1 \times 10^{-2}$ m^2 s^{-1}. While incorporating variation with stratification improves the overall fit, both methods are statistically significant, suggesting that using a constant K_Z (which may be easier to apply in some situations) would be acceptable. This is further explored in section 4. The values of K_z reported here fall within the range of values of eddy diffusivity observed previously in river plumes [typically from $O(10^{-4})$ to $O(10^{-2})$ m^2 s^{-1}] (MacDonald and Geyer 2004; McCabe et al. 2008). These are the first estimates of the vertical eddy diffusivity of salt in the surf zone, where prior studies in the absence of a river plume have shown lateral dispersion to be dominant (Clark et al. 2010; Spydell and Feddersen 2012; Hally-Rosendahl et al. 2014).

4. Discussion

a. Tidal dependence of stratification and mixing

While a constant value of eddy diffusivity K_z statistically significantly models the mixing of the Quinault plume in the surf zone, calculations of eddy diffusivity using bin-averaged values of vertical salt flux and stratification have a range of one order of magnitude (section 3c; Fig. 8b). To determine the source of this variability, we examine tidal influence on river volume flux [Q_T in Eq. (5)] and surf-zone stratification (Figs. 9a,b). Of relevance here is that Q_T is a maximum at low water and a minimum at high water because of estuarine storage.

The tidal dependence of stratification shown in Fig. 3g indicates that surf-zone stratification increases as the input freshwater flux decreases with increasing tidal stage. One implication of this increasing stratification is that the surf zone near the river mouth loses freshwater content due to a net export of freshwater. A loss of freshwater content near the river mouth could be caused by several processes: the export of surf-zone-trapped freshwater to the inner shelf, alongshore plume spreading and thinning in the surf zone, a change in the volume of the surf zone without a corresponding increase in freshwater, or mixing. These processes are impossible to distinguish with Lagrangian measurements, but mixing seems unlikely to be a significant contributor due to the increase in near-surface stratification with tidal stage. Mixing that reduces the freshwater content of a river plume is typically associated with a deepening pycnocline and decreasing near-surface stratification, the opposite of what we observe (Fong and Geyer 2001; Lentz 2004; McCabe et al. 2008).

Possible transport mechanisms for freshwater in the surf zone include alongshore current and rip current (transient or bathymetric) driven transport (Reniers et al. 2009; Kumar and Feddersen 2017b; Grimes et al. 2020). Alongshore dispersion is high in the surf zone ($0.1 < K_y < 10$ m^2 s^{-1}) (Spydell and Feddersen 2009; Clark et al. 2010; Hally-Rosendahl et al. 2014), and transport of river water within the surf zone by an alongshore current will have important implications for coastal public health, ecology, and morphodynamics and is addressed in some previous studies (Wong et al. 2013; Rodriguez et al. 2018). For constant wave height and angle of approach, the volume transport due to wave-driven alongshore currents would be largest at low water and minimum at high water due to the tidal influence on surf-zone width (which would be largest at low water under the same

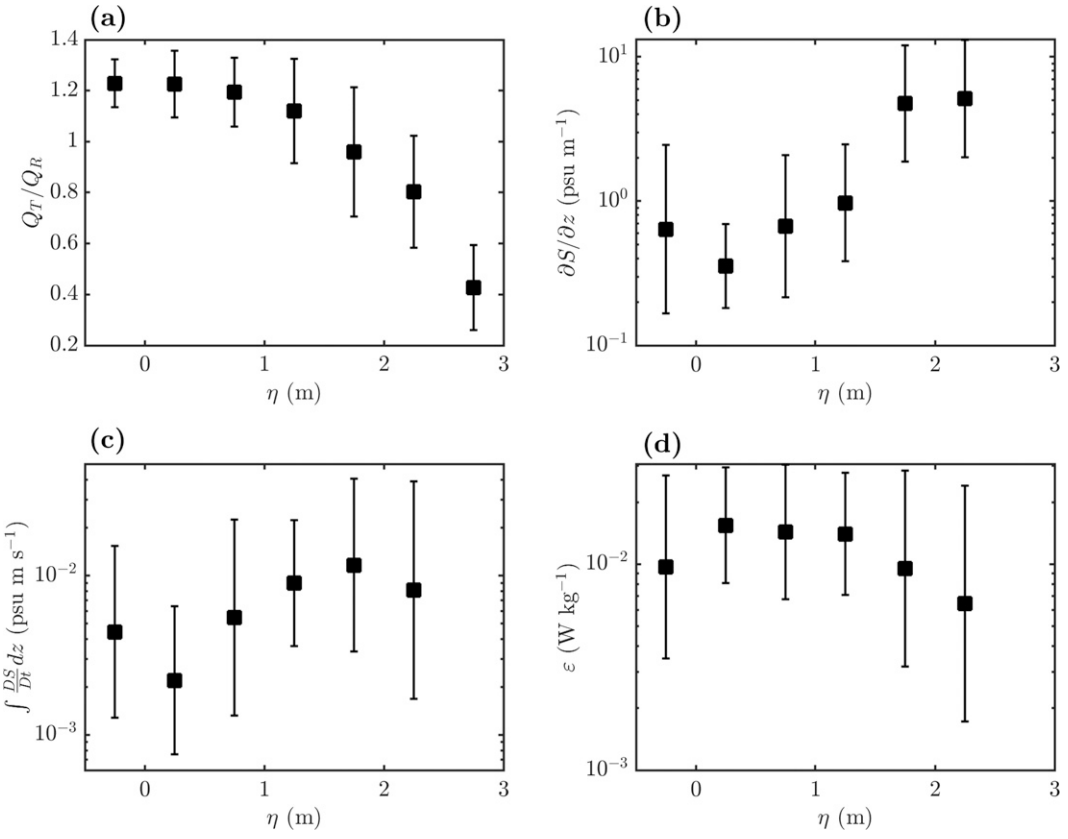

FIG. 9. River volume flux, stratification, and salt flux depend on tidal stage η, whereas TKE dissipation rate does not: (a) volume flux at the mouth Q_T normalized by upstream river discharge Q_R, decreasing with tidal stage η, calculated as described in Eq. (5) and Kastner et al. (2019); (b) stratification $\partial S/\partial z$, increasing with tidal stage (averages of SWIFTv3 1-min estimates); (c) salt flux $\int (DS/Dt)\, dz$, increasing with tidal stage (averages of SWIFTv3 1-min estimates); and (d) TKE dissipation rate ε, with no clear trend with respect to tidal stage (averages of SWIFTv3 and SWIFTv4 1-min estimates). Black squares are bin averages in 0.5-m tidal stage bins of the relevant quantity, with an error bar showing the standard deviation. Statistics are calculated in linear space for volume flux [in (a)] and log space for all other quantities [(b)–(d)].

wave conditions due to the Quinault River mouth bathymetry). Interestingly, river volume flux has the same phasing relative to the tide: maximum at high water and minimum at low water. We address potential lateral mixing that may result from these processes in the next section.

While we have not directly included the contribution of plume spreading to stratification changes in this analysis, we estimate the vertical advective velocity associated with plume spreading to be small (section 2b). This estimate does not directly address the possible shoreward advection of a sloping isohaline that is deepest at the river mouth and surfaces offshore. Such advection would lead to an increase in near surface stratification near the river mouth as saltwater from the inner shelf enters the surf zone. Onshore directed tidal currents could cause this advection pattern, which would be balanced by alongshore transport of plume water and/or export of plume water to the inner shelf if the volume of the surf zone did not change with the tide (i.e., on a planar beach with a constant wave field). Notably, on 30 April 2017, the wave height happens to increase with the tidal stage, resulting in an increase in the surf-zone volume (Fig. 5; Table 2). This is a special case that does not require a balancing freshwater flux in order for onshore advection to increase stratification. We therefore hypothesize that the loss of surf-zone freshwater content is driven by a combination of alongshore transport of plume water in the surf zone, export of freshwater to the inner shelf, and advection of the surf-zone density gradient.

Figure 9a shows river volume flux normalized by estimated river discharge binned as a function of tidal stage. Normalized river volume flux decreases with tidal stage, while stratification in the upper 1.05 m of the surf zone increases with tidal stage, as on 30 April 2017 (Figs. 3 and 9b). We caution the reader that the quasi-Lagrangian SWIFT measurements do not straightforwardly represent the surf-zone-wide stratification; we mitigate this by leveraging both short, repeated drifts (as shown in Fig. 2) and the recirculating nature of the drift shown in Fig. 3. All of these drifts remain in the surf zone and thus primarily elucidate changes in stratification and salt flux over increasing tidal stage and the associated decreasing freshwater flux. Both mixing rate and the vertically integrated

mixing rate increase with increasing tidal stage, especially for $0 < \eta < 2$ m (Fig. 9c). Thus, stratification and salt flux increase as river volume flux decreases. In turn, the values of eddy diffusivity calculated by dividing the bin-averaged vertically integrated mixing rate (taken as the vertical salt flux as explained in section 2b) by the stratification [Eq. (3)] decrease with increasing tidal stage as stratification increases and river volume flux decreases (Fig. 8b). TKE dissipation rate in the upper 0.5 m decreases slightly with tidal stage (Fig. 9d), possibly suggesting the suppression of turbulence as stratification increases with tidal stage. This is addressed more directly in section 4c.

Taken together, the dependencies described above suggest that mixing is inhibited when the surf zone is highly stratified, analogous with the general understanding that stratification inhibits vertical mixing (Thorpe 1973). Specifically, our results are similar to previous estuarine studies that use a reduced eddy diffusivity during high stratification to represent turbulence suppression due to stratification (e.g., Stacey and Ralston 2005; MacCready 2007). The order-of-magnitude decrease in eddy diffusivity in conjunction with a two-order-of-magnitude increase in stratification results in a one-order-of-magnitude increase in vertical salt flux, indicating that, despite inhibited eddy diffusivity at high stratification, vertical salt flux still increases with increasing stratification. The observed decrease in eddy diffusivity is therefore a second-order effect in comparison with the observed increase in salt flux supported by the presence of increased stratification.

b. *Lateral mixing in the surf zone*

For lateral mixing of a river plume in the surf zone to occur there must be both lateral velocity fluctuations and a lateral gradient of salinity within the surf zone. As noted above, lateral diffusivity in the surf zone has been found to be $0.1 < K_x < 10\ \mathrm{m^2\ s^{-1}}$ (Spydell and Feddersen 2009; Clark et al. 2010; Hally-Rosendahl et al. 2014), indicating the presence of significant lateral velocity fluctuations. Therefore, lateral mixing of a river plume in the surf zone will primarily depend on the lateral salinity gradients present. Figure 7 shows that the offshore mooring salinity is on average much higher than that measured by the SWIFTs in the surf zone. The cross-shore salinity gradient, which is expected to be higher than the alongshore gradient due to the bounding influence of the surf-zone edge, is therefore primarily dependent on the cross-shore salinity structure inside the surf zone.

The observed cross-shore salinity structure in the surf zone is dependent on the tidal stage (Fig. 10). For $\eta < 1.5$ m, the surf zone is very fresh throughout its cross-shore extent, with evidence of a slight increase in salinity toward the edge of the surf zone (Figs. 10a,b). There is therefore a sharp salinity gradient at the edge of the surf zone when $\eta < 1.5$ m; this is a likely location where lateral mixing is important. The cross-shore salt flux can be scaled as $\overline{S'u'} \sim K_x \partial S/\partial x$, where the salinity gradient at the edge of the surf zone is $\partial S/\partial x \sim O(10^{-1})$ psu $\mathrm{m^{-1}}$. Using $10^{-1} < K_x < 10^{1}\ \mathrm{m^2\ s^{-1}}$, we find that $10^{-2}\overline{S'u'} \sim 10^{0}$psu m $\mathrm{s^{-1}}$, ranging between values that are comparable to the values of vertical salt flux estimated from the SWIFTs at low water and midwater to two orders of magnitude higher. The salt flux associated with mixing at the edge of the surf zone acts through an area defined by the length scales d_b (the breaker depth) and L_y (the alongshore extent of the plume). Meanwhile, vertical mixing acts through the bottom of the plume, defined by L_y and L_{SZ}. The area through which vertical mixing acts is therefore larger than the area through which lateral mixing acts by a factor of $L_{SZ}/d_b \approx O(10^2)$. So, although the lateral salt fluxes may be as large as the vertical salt fluxes, the net effect of vertical mixing will be larger (except for large values of K_x) as vertical mixing acts over a larger area. At low water and midwater, lateral mixing will also be most important at the edge of the surf zone; during the recirculating drift on 30 April 2017, the SWIFTs stayed in the surf-zone interior and therefore experience minimal influence of lateral mixing at low water and midwater (section 3b), regardless of K_x.

When $\eta > 1.5$ m, there is a significant cross-shore gradient of salinity in the surf zone, and the above assumption that all lateral mixing occurs at the edge of the surf zone is no longer

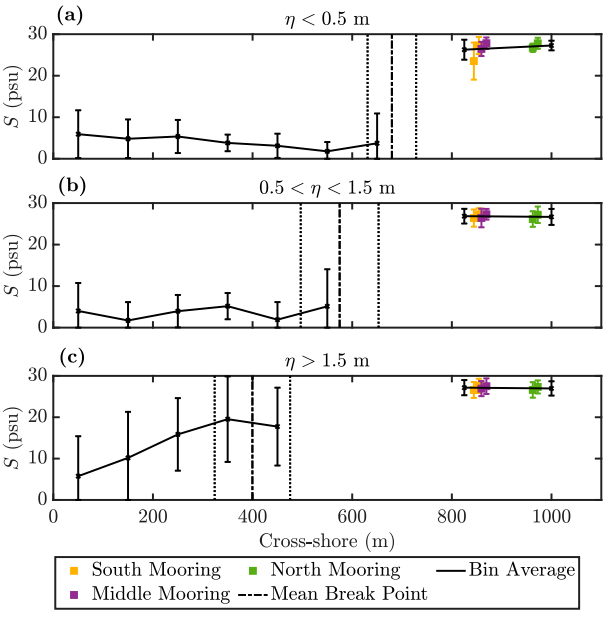

FIG. 10. Cross-shore profiles of quantities measured from trapped SWIFT drifters and nearshore moorings at alongshore positions less than 1500 m from the river mouth when tidal stage from the USGS Point Grenville gauge is (a) less than 0.5 m above mean lower low water (MLLW), (b) between 0.5 and 1.5 m MLLW, and (c) greater than 1.5 m MLLW. Each panel shows a cross-shore bin average of salinity with a bin size of 100 m; the error bars represent the standard deviation of salinity in each bin. The deployment-average salinity for the nearshore moorings is also shown, with error bars indicating standard deviation. Salinity measurements from all surf-zone-trapped SWIFT drifters within the space and time constraints are included (see Table 2 for measurement depths). There are two points for each mooring, offset in the horizontal for clarity; the fresher point for each mooring is the 1-m CTD, and the saltier point is the 3-m CTD. The mean surf-zone width (m) for each tidal bin is given by the black dashed vertical line, with the black dotted lines indicating 1 standard deviation from the mean break point.

valid (Fig. 10c). The cross-shore salinity gradient at high water is $\partial S/\partial x \sim O(10^{-2})$ psu m^{-1}. In section 3c we introduced the fitting intercept $\mathscr{C}$ in our mixing estimate [Eq. (6)]; if we assume that $\mathscr{C} = 5.8 \times 10^{-3}$ psu m s^{-1} solely describes lateral mixing, then we can estimate the cross-shore eddy diffusivity of salt as $K_x \approx O(10^{-1})$ m^2 s^{-1}, consistent with the lower values found in previous studies (we use this approximate value of K_x in the scaling that follows). So, $\mathscr{C}$ may reasonably describe lateral mixing at high water; this leaves the question: how important is lateral mixing relative to vertical mixing at high water? When $\eta > 1.5$, the average vertically integrated mixing rate we estimate from the SWIFTs is $\int(DS/Dt)\,dz \approx O(10^{-2})$ psu m s^{-1}, larger than the horizontal salt flux obtained by multiplying $K_x \sim 10^{-1}$ m^2 s^{-1} by the previously reported cross-shore salinity gradient within the surf zone, $\overline{S'u'} \sim O(10^{-3})$ psu m s^{-1}.

In summary, lateral mixing may play a role in mixing a river plume in the surf zone when there is a significant cross-shore salinity gradient within the surf zone. At the Quinault River mouth, this condition occurs at high water, as the tidal volume flux of freshwater is at its minimum and the remaining freshwater in the surf zone is concentrated in a near-surface layer. We estimate that lateral mixing is on average less important than vertical mixing during high water at the Quinault River mouth, but the extent to which this is true at any given time will depend on the surf-zone cross-shore salinity gradient and stratification. At lower tidal stages, we do not observe a significant cross-shore salinity gradient within the surf zone, and the impact of lateral mixing at the surf-zone–inner-shelf boundary where salinity gradients are high is inhibited by the small cross-shore area it acts through at the edge of the surf zone. Lateral mixing will likely be important at the edge of the surf zone under such conditions; the drifters we deployed at the Quinault River mouth did not preferentially sample the surf-zone edge (section 3b; Fig. 5).

c. *Stratified turbulence in the surf zone*

Our turbulent dissipation rate estimates, while in agreement with the bulk formulation presented in section 2b, are noisy and do not resolve variability on the spatial scales associated with stratification in the top 1.05 m of the surf zone (we make dissipation estimates in the top 0.5 m). We therefore cannot directly assess the degree to which turbulence is suppressed by high stratification; however, it is still useful to explore the parameter space of stratified turbulence in the surf zone based on the order of magnitude of the observed quantities. We expect that the mixing behavior of river plumes in the surf zone may be different than many other stratified turbulence processes in nature because the wave-driven turbulence is generated independently from the river-supplied stratification. We frame this exploration with two main questions: Can high surf-zone stratification suppress turbulence and mixing? How do we interpret the lack of a relationship between salt flux and TKE dissipation rate?

Trends in TKE dissipation rate in both ensemble-averaged and individual drifts are weaker than trends in vertical salt flux and stratification (Figs. 2e, 3e, and 6d). We will therefore use the range of ensemble-averaged dissipation values presented in Fig. 6d, $10^{-3} < \varepsilon < 10^{-2}$ W kg^{-1} (after correcting for high void fraction) in the remainder of our analysis. This range of turbulent dissipation rates is consistent with previous surf-zone studies (George et al. 1994; Feddersen and Trowbridge 2005; Feddersen 2012a).

The Ozmidov length scale L_O characterizes the vertical length scale at which the energy contained in turbulent eddies is suppressed by stratification, and can be calculated (for salinity stratification) as

$$L_O = \sqrt{\frac{\varepsilon}{\left(g\beta\frac{\partial S}{\partial z}\right)^{3/2}}}, \tag{7}$$

where $\beta = 0.77 \times 10^{-3}$ psu^{-1} is the haline contraction coefficient (Turner 1973). Short-time-scale estimates of L_O using the SWIFT data are noisy, but we can constrain its range using order-of-magnitude approximations for near-surface TKE dissipation rate and stratification. Using $10^{-3} < \varepsilon < 10^{-2}$ W kg^{-1} as a representative range of TKE dissipation rates as $\partial S/\partial z$ varies from 10^{-1} to 10^{1} psu m^{-1}, we find $10^{-1} < L_O < 10^{1}$ m. The lower end of these values is similar to estimates of near-surface L_O in the Columbia and Fraser River plumes ($L_O \sim 10^{-1}$ m; MacDonald and Geyer 2004; Nash et al. 2009). When stratification is high, L_O can be an order-of-magnitude less than 1.05 m, the depth of the deepest salinity measurement on the SWIFTv3 (Table 1). Taking 1.05 m to be representative of the distance from our measurements to the boundary, this supports the conclusion that near-surface turbulence may be suppressed by stratification. Conversely, when surf-zone stratification is low, L_O is much larger than 1.05 m, and turbulence may not be influenced by stratification. Thus, the observed range of Ozmidov scales suggests that the strength of stratification during periods of high stratification may be sufficient to influence turbulence. This is consistent with our finding that K_z is smaller when stratification is high. We note that high near-surface stratification could be the result of the plume interface becoming shallower. This would expose the large vertical salinity gradient at the interface to stronger wave-breaking driven turbulence near the water surface; this mechanism is similar to that described in Gerbi et al. (2015) for whitecapping-driven plume mixing.

Vertical salt flux is related to TKE dissipation rate through the mixing efficiency Γ according to

$$\Gamma\varepsilon = -g\beta\int\frac{DS}{Dt}\,dz, \tag{8}$$

where the right side of the equation is the buoyancy flux $\mathscr{B}$ expressed in terms of the salinity (Turner 1973). Using Eqs. (1) and (8) and the values of ε and DS/Dt used above in estimates of L_O, we would expect mixing efficiency values in the range of $10^{-4} < \Gamma < 10^{-1}$. This broad range includes values similar to literature values for shear-driven mixing efficiency (Ivey and Imberger 1991; Gregg 2004) ($\Gamma \sim 0.2$), but mixing efficiencies are often lower by an order of magnitude or more. While the reasons for this cannot be discerned with our observations, it is plausible that wave-breaking turbulence is less effective than shear generated turbulence at generating buoyancy flux because the turbulence generation process is dislocated from the mixing

processes. Moreover, the manner in which stratification controls turbulence generation and evolution in each scenario differs. Notably, the Ozmidov length scales we estimate above suggest that the evolution of this turbulence may still be impacted by the presence of stratification. The impact of the dislocation of turbulence generation from stratification may be similar to laboratory studies of grid-generated turbulence, where mixing efficiency in the form of the flux Richardson number has been shown to have a maximum of 0.06, with values as low as $O(10^{-3})$ observed in several studies (Rehmann 2004; Stretch et al. 2010).

d. Comparison with conventional river plumes

In a saturated surf zone, where all waves break and depth-averaged TKE dissipation rate is primarily a function of bathymetry, local TKE dissipation rate does not depend on offshore wave forcing (Wright et al. 1982; Raubenheimer et al. 1996). This decoupling of forcing and dissipation is unlike the stratified shear turbulence common to most river plume studies, where an increase in tidal river mouth velocity typically leads to an increase in shear and can increase the TKE dissipation rate at the pycnocline if stratification is sufficiently low, causing mixing (Nash et al. 2009; MacDonald et al. 2007; Jurisa et al. 2016). In a saturated surf zone, therefore, we expect dissipation to always be high enough to cause mixing, depending on the local bathymetry but not necessarily on the offshore wave condition.

The range of vertical salt flux values shown in Fig. 8 correspond to buoyancy flux values that vary from 10^{-6} to 10^{-4} W kg^{-1}. This range spans observations from other river plumes; the upper values ($\mathscr{B} \sim 10^{-4}$ W kg^{-1}) are similar to the buoyancy fluxes observed in the near-field Fraser River plume (MacDonald and Geyer 2004), the moderate values ($\mathscr{B} \sim 10^{-5}$ W kg^{-1}) are similar to those observed in the near-field Columbia River plume (McCabe et al. 2008), and the lower values ($\mathscr{B} \sim 10^{-6}$ W kg^{-1}) are similar to the midfield Columbia River plume (McCabe et al. 2008) and larger than buoyancy fluxes observed in the far-field Chesapeake Bay plume (Fisher et al. 2018) ($\mathscr{B} \leq 10^{-7}$ W kg^{-1}). The buoyancy fluxes observed in these other plume systems are related to their proximity to the river mouth, and therefore depend on quantities such as river discharge, stratification, and velocity shear. We observe similar dependencies in the surf zone at the Quinault River mouth; tidal modulation of river volume flux changes the surf-zone stratification, vertical eddy diffusivity, and buoyancy flux.

The highest estimates of vertical salt flux at the Quinault occur at high water when near-surface surf-zone stratification is highest. This is also when the tidal river mouth velocity and volume flux are lowest (Kastner et al. 2019). Therefore, as the river mouth velocity decreases, the freshwater that remains near the river mouth is more and more surface concentrated and becomes exposed to surface-intensified wave-breaking turbulence. The timing of maximum salt flux in the surf zone at the Quinault River mouth is thus opposite the timing of maximum salt flux at the Columbia River mouth, where the highest salt fluxes are associated with maximum tidal velocity (Nash et al. 2009). This difference highlights the importance of the turbulence generation mechanism to mixing behavior. We do observe that stratification can suppress the mixing of the Quinault River plume in the surf zone, as eddy diffusivity decreases when stratification is high. This is a more minor impact than in Nash et al. (2009), where high stratification during periods of low tidal velocity can shut down mixing entirely.

5. Summary

We present results from an observational study of river plume mixing in the surf zone near the Quinault River mouth. Salinity measurements from SWIFT drifters document the presence of the plume in the surf zone, which is fresher than the inner shelf. Notably, we also observe that the surf zone is often strongly stratified, even in the presence of energetic wave breaking. We show that plume mixing, quantified based on the vertical salt flux, varies with the tide; however, the TKE dissipation rate does not depend on either the tidal elevation or the wave height. Instead, we find that the vertical salt flux is controlled by the strength of the near-surface stratification:

- At low water (maximum ebb) the river volume flux is high, the surf zone is often filled with freshwater, stratification is low, and therefore vertical salt flux is low despite high ε.
- Near high water (close to maximum flood), freshwater volume flux is low, the surf zone becomes stratified, and the combination of persistently high wave-breaking turbulence with the high stratification results in high vertical salt flux.

It is likely that stratification and mixing will depend on wave height at times of year when the wave height is much smaller, but no dependence is observed during the typical springtime conditions during our study, which usually resulted in a stratified surf zone.

The average value of the vertical eddy diffusivity during the experiment was found to be $K_z \approx (2.2 \pm 0.6) \times 10^{-3}$ m^2 s^{-1} based on the relationship between stratification and vertical salt flux, with a range of $1.4 \times 10^{-3} < K_z < 1 \times 10^{-2}$. We observe that lower K_z values are associated with higher stratification, suggesting that stratification may suppress wave-driven turbulent mixing. However, the large dynamic range of stratification still causes vertical salt flux to monotonically increase with stratification, indicating that the decrease in eddy diffusivity is a second-order effect on surf-zone river plume mixing.

Acknowledgments. This work would not have been possible without the advice and consent of the Quinault Indian Nation, particularly the Quinault Division of Natural Resources and Quinault River Committee. Specifically, we thank Joe Shumacker, Larry Gilbertson, Kokomo Snell, and Kristen Phillips. Additionally, this project is supported, in part, by National Science Foundation Grants OCE-1459051, OCE-1923941, and OCE-1924005. Melissa Moulton, Alex De Klerk, and Joe Talbert provided significant assistance with the UAS, buoys, and moorings. Joel Corlew, Raul Flores, Andy Reay-Ellers, Avery Snyder, and Seth Zippel from the University of Washington Environmental Fluid Mechanics group and Applied Physics Laboratory also assisted with fieldwork. Melissa Moulton and Parker MacCready provided valuable feedback. Spirited discussions with Nirnimesh Kumar were critical to this

TABLE A1. All SWIFT deployments that resulted in the drifters being trapped at the river mouth. The date and UTC time of the deployment are given for each drift, as is the model of SWIFT deployed (see Table 1), the tidal stage from the USGS Point Grenville station in meters, and the significant wave height from the offshore AWAC wave measurement The AWAC was removed on 3 May 2017, resulting in missing wave height data ("N/A") at the end of the record in the table.

Date (2017)	Time (UTC)	SWIFT model	η (m)	H_S (m)
26 Apr	2236	3	1.81	1.95
27 Apr	1825	3	1.30	1.95
27 Apr	1935	3	2.00	1.94
27 Apr	2124	3	2.45	1.88
27 Apr	2126	3	2.44	1.87
27 Apr	2212	4	2.30	1.83
27 Apr	2324	4	1.85	1.76
28 Apr	1909	4	1.18	1.48
28 Apr	1925	3	1.34	1.50
28 Apr	1931	3	1.37	1.51
28 Apr	2109	4	2.24	1.59
28 Apr	2112	4	2.25	1.59
28 Apr	2124	3	2.29	1.54
28 Apr	2127	3	2.30	1.54
28 Apr	2327	3	2.15	1.40
29 Apr	2112	4	1.83	1.12
29 Apr	2112	3	1.83	1.12
29 Apr	2248	4	2.30	1.25
30 Apr	1724	4	−0.41	1.57
30 Apr	1728	3	−0.41	1.57
30 Apr	2100	3	1.16	2.04
1 May	1700	3	0.02	1.42
1 May	1700	3	0.02	1.42
1 May	1915	3	−0.13	1.25
2 May	1600	3	1.14	1.25
2 May	1603	3	1.14	1.25
2 May	1700	3	0.57	1.35
2 May	1703	3	0.57	1.35
2 May	1836	3	0.00	1.35
2 May	1839	3	0.00	1.35
3 May	2212	3	0.40	N/A
4 May	1724	4	1.50	N/A
4 May	1726	4	1.50	N/A
4 May	1900	4	0.83	N/A
4 May	1933	4	0.60	N/A
5 May	1800	3	1.71	N/A

work; he is missed dearly. Jody Klymak, Nicole Jones, Falk Feddersen, and three anonymous reviewers provided helpful critiques of this paper and its previous iteration.

Data availability statement. Data are available online (https://digital.lib.washington.edu/researchworks/handle/1773/15609).

APPENDIX

Surf-Zone-Trapped SWIFT Deployments

Table A1 gives the details of the deployment time, model, tidal stage, and wave height for all SWIFT deployments that resulted in surf-zone-trapped drifters.

REFERENCES

Akan, Ç., S. Moghimi, H. T. Özkan-Haller, J. Osborne, and A. Kurapov, 2017: On the dynamics of the mouth of Columbia River: Results from a three-dimensional fully coupled wave-current interaction model. *J. Geophys. Res. Oceans*, **122**, 5218–5236, https://doi.org/10.1002/2016JC012307.

Battjes, J. A., and J. P. F. M. Janssen, 1978: Energy loss and set-up due to breaking of random waves. *16th Int. Conf. on Coastal Engineering*, Hamburg, Germany, American Society of Civil Engineers, 32 pp., https://doi.org/10.1061/9780872621909.034.

Bowen, A. J., and R. A. Holman, 1989: Shear instabilities of the mean longshore current: 1. Theory. *J. Geophys. Res.*, **94**, 18 023–18 030, https://doi.org/10.1029/JC094iC12p18023.

Chen, F., and D. G. MacDonald, 2006: Role of mixing in the structure and evolution of a buoyant discharge plume. *J. Geophys. Res.*, **111**, C11002, https://doi.org/10.1029/2006JC003563.

Clark, D. B., F. Feddersen, and R. T. Guza, 2010: Cross-shore surfzone tracer dispersion in an alongshore current. *J. Geophys. Res.*, **115**, C10035, https://doi.org/10.1029/2009JC005683.

——, S. Elgar, and B. Raubenheimer, 2012: Vorticity generation by short-crested wave breaking. *Geophys. Res. Lett.*, **39**, L24604, https://doi.org/10.1029/2012GL054034.

Dalrymple, R. A., 1975: A mechanism for rip current generation on an open coast. *J. Geophys. Res.*, **80**, 3485–3487, https://doi.org/10.1029/JC080i024p03485.

Derakhti, M., J. Thomson, and J. T. Kirby, 2020: Sparse sampling of intermittent turbulence generated by breaking surface waves. *J. Phys. Oceanogr.*, **50**, 867–885, https://doi.org/10.1175/JPO-D-19-0138.1.

Feddersen, F., 2012a: Observations of the surfzone turbulent dissipation rate. *J. Phys. Oceanogr.*, **42**, 386–399, https://doi.org/10.1175/JPO-D-11-082.1.

——, 2012b: Scaling surf zone turbulence. *Geophys. Res. Lett.*, **39**, L18613, https://doi.org/10.1029/2012GL052970.

——, 2014: The generation of surfzone eddies in a strong alongshore current. *J. Phys. Oceanogr.*, **44**, 600–617, https://doi.org/10.1175/JPO-D-13-051.1.

——, and J. H. Trowbridge, 2005: The effect of wave breaking on surf-zone turbulence and alongshore currents: A modeling study. *J. Phys. Oceanogr.*, **35**, 2187–2203, https://doi.org/10.1175/JPO2800.1.

——, ——, and A. J. Williams III, 2007: Vertical structure of dissipation in the nearshore. *J. Phys. Oceanogr.*, **37**, 1764–1777, https://doi.org/10.1175/JPO3098.1.

Fisher, A. W., N. J. Nidzieko, M. E. Scully, R. J. Chant, E. J. Hunter, and P. L. F. Mazzini, 2018: Turbulent mixing in a far-field plume during the transition to upwelling conditions: Microstructure observations from an AUV. *Geophys. Res. Lett.*, **45**, 9765–9773, https://doi.org/10.1029/2018GL078543.

Fong, D. A., and W. R. Geyer, 2001: Response of a river plume during an upwelling favorable wind event. *J. Geophys. Res.*, **106**, 1067–1084, https://doi.org/10.1029/2000JC900134.

George, R., R. E. Flick, and R. T. Guza, 1994: Observations of turbulence in the surf zone. *J. Geophys. Res.*, **99**, 801–810, https://doi.org/10.1029/93JC02717.

Gerbi, G. P., J. H. Trowbridge, E. A. Terray, A. J. Plueddemann, and T. Kukulka, 2009: Observations of turbulence in the ocean surface boundary layer: Energetics and transport. *J. Phys. Oceanogr.*, **39**, 1077–1096, https://doi.org/10.1175/2008JPO4044.1.

——, R. J. Chant, and J. L. Wilkin, 2013: Breaking surface wave effects on river plume dynamics during upwelling-favorable

winds. *J. Phys. Oceanogr.*, **43**, 1959–1980, https://doi.org/10.1175/JPO-D-12-0185.1.

——, S. E. Kastner, and G. Brett, 2015: The role of whitecapping in thickening the ocean surface boundary layer. *J. Phys. Oceanogr.*, **45**, 2006–2024, https://doi.org/10.1175/JPO-D-14-0234.1.

Geyer, W. R., A. C. Lavery, M. E. Scully, and J. H. Trowbridge, 2010: Mixing by shear instability at high Reynolds number. *Geophys. Res. Lett.*, **37**, L22607, https://doi.org/10.1029/2010GL045272.

——, D. K. Ralston, and R. C. Holleman, 2017: Hydraulics and mixing in a laterally divergent channel of highly stratified estuary. *J. Geophys. Res. Oceans*, **122**, 4743–4760, https://doi.org/10.1002/2016JC012455.

Gregg, M. C., 2004: Small-scale processes in straits. *Deep-Sea Res. II*, **51**, 489–503, https://doi.org/10.1016/j.dsr2.2003.08.003.

Grimes, D. J., F. Feddersen, and N. Kumar, 2020: Tracer exchange across the stratified inner-shelf driven by transient rip-currents and diurnal surface heat fluxes. *Geophys. Res. Lett.*, **47**, e2019GL086501, https://doi.org/10.1029/2019GL086501.

Haller, M. C., U. Putrevu, J. Oltman-Shay, and R. A. Dalrymple, 1999: Wave group forcing of low frequency surf zone motion. *Coastal Eng. J.*, **41**, 121–136, https://doi.org/10.1142/S0578563499000085.

Hally-Rosendahl, K., and F. Feddersen, 2016: Modeling surfzone to inner-shelf tracer exchange. *J. Geophys. Res. Oceans*, **121**, 4007–4025, https://doi.org/10.1002/2015JC011530.

——, ——, and R. T. Guza, 2014: Cross-shore tracer exchange between the surfzone and inner-shelf. *J. Geophys. Res. Oceans*, **119**, 4367–4388, https://doi.org/10.1002/2013JC009722.

Hetland, R. D., 2010: The effects of mixing and spreading on density in near-field river plumes. *Dyn. Atmos. Oceans*, **49**, 37–53, https://doi.org/10.1016/j.dynatmoce.2008.11.003.

Hickey, B. M., and Coauthors, 2010: River influences on shelf ecosystems: Introduction and synthesis. *J. Geophys. Res.*, **115**, C00B17, https://doi.org/10.1029/2009JC005452.

Horner-Devine, A. R., R. D. Hetland, and D. G. MacDonald, 2015: Transport and mixing in coastal river plumes. *Annu. Rev. Fluid Mech.*, **47**, 569–594, https://doi.org/10.1146/annurev-fluid-010313-141408.

Ivey, G. N., and J. Imberger, 1991: On the nature of turbulence in a stratified fluid. I: The energetics of mixing. *J. Phys. Oceanogr.*, **21**, 650–658, https://doi.org/10.1175/1520-0485(1991)021<0650:OTNOTI>2.0.CO;2.

Izett, J. G., and K. Fennel, 2018: Estimating the cross-shelf export of riverine materials: Part 2. Estimates of global freshwater and nutrient export. *Global Biogeochem. Cycles*, **32**, 176–186, https://doi.org/10.1002/2017GB005668.

Jennings, W. C., S. Cunniff, K. Lewis, H. Deres, D. R. Reineman, J. Davis, and A. B. Boehm, 2020: Participatory science for coastal water quality: Freshwater plume mapping and volunteer retention in a randomized informational intervention. *Environ. Sci.: Processes Impacts*, **22**, 918–929, https://doi.org/10.1039/C9EM00571D.

Jurisa, J. T., J. D. Nash, J. N. Moum, and L. F. Kilcher, 2016: Controls on turbulent mixing in a strongly stratified and sheared tidal river plume. *J. Phys. Oceanogr.*, **46**, 2373–2388, https://doi.org/10.1175/JPO-D-15-0156.1.

Kakoulaki, G., D. MacDonald, and A. R. Horner-Devine, 2014: The role of wind in the near field and midfield of a river plume. *Geophys. Res. Lett.*, **41**, 5132–5138, https://doi.org/10.1002/2014GL060606.

Kastner, S. E., A. R. Horner-Devine, and J. Thomson, 2018: The influence of wind and waves on spreading and mixing in the Fraser River plume. *J. Geophys. Res. Oceans*, **123**, 6818–6840, https://doi.org/10.1029/2018JC013765.

——, ——, and J. M. Thomson, 2019: A conceptual model of a river plume in the surf zone. *J. Geophys. Res. Oceans*, **124**, 8060–8078, https://doi.org/10.1029/2019JC015510.

Kilcher, L. F., J. D. Nash, and J. N. Moum, 2012: The role of turbulence stress divergence in decelerating a river plume. *J. Geophys. Res.*, **117**, C05032, https://doi.org/10.1029/2011JC007398.

Kumar, N., and F. Feddersen, 2017a: The effect of stokes drift and transient rip currents on the inner shelf. Part I: No stratification. *J. Phys. Oceanogr.*, **47**, 227–241, https://doi.org/10.1175/JPO-D-16-0076.1.

——, and ——, 2017b: The effect of stokes drift and transient rip currents on the inner shelf. Part II: With stratification. *J. Phys. Oceanogr.*, **47**, 243–260, https://doi.org/10.1175/JPO-D-16-0077.1.

Lentz, S., 2004: The response of buoyant coastal plumes to upwelling-favorable winds. *J. Phys. Oceanogr.*, **34**, 2458–2469, https://doi.org/10.1175/JPO2647.1.

Longuet-Higgins, M. S., and R. W. Stewart, 1962: Radiation stress and mass transport in gravity waves, with application to 'surf beats.' *J. Fluid Mech.*, **13**, 481–504, https://doi.org/10.1017/S0022112062000877.

Lund, B., H. C. Graber, P. O. G. Persson, M. Smith, M. Doble, J. Thomson, and P. Wadhams, 2018: Arctic sea ice drift measured by shipboard marine radar. *J. Geophys. Res. Oceans*, **123**, 4298–4321, https://doi.org/10.1029/2018JC013769.

MacCready, P., 2007: Estuarine adjustment. *J. Phys. Oceanogr.*, **37**, 2133–2145, https://doi.org/10.1175/JPO3082.1.

——, W. R. Geyer, and H. Burchard, 2018: Estuarine exchange flow is related to mixing through the salinity variance budget. *J. Phys. Oceanogr.*, **48**, 1375–1384, https://doi.org/10.1175/JPO-D-17-0266.1.

MacDonald, D. G., and W. R. Geyer, 2004: Turbulent energy production and entrainment at a highly stratified estuarine front. *J. Geophys. Res.*, **109**, C05004, https://doi.org/10.1029/2003JC002094.

——, L. Goodman, and R. D. Hetland, 2007: Turbulent dissipation in a near-field river plume: A comparison of control volume and microstructure observations with a numerical model. *J. Geophys. Res.*, **112**, C07026, https://doi.org/10.1029/2006JC004075.

MacMahan, J. H., A. J. H. M. Reniers, E. B. Thornton, and T. P. Stanton, 2004: Surf zone eddies coupled with rip current morphology. *J. Geophys. Res.*, **109**, C07004, https://doi.org/10.1029/2003JC002083.

McCabe, R. M., B. M. Hickey, and P. MacCready, 2008: Observational estimates of entrainment and vertical salt flux in the interior of a spreading river plume. *J. Geophys. Res.*, **113**, C08027, https://doi.org/10.1029/2007JC004361.

Moghimi, S., J. Thomson, T. Özkan-Haller, L. Umlauf, and S. Zippel, 2016: On the modeling of wave-enhanced turbulence nearshore. *Ocean Modell.*, **103**, 118–132, https://doi.org/10.1016/j.ocemod.2015.11.004.

Moulton, M., S. Elgar, B. Raubenheimer, J. C. Warner, and N. Kumar, 2017: Rip currents and alongshore flows in single channels dredged in the surf zone. *J. Geophys. Res. Oceans*, **122**, 3799–3816, https://doi.org/10.1002/2016JC012222.

Nash, J. D., and J. N. Moum, 2005: River plumes as a source of large-amplitude internal waves in the coastal ocean. *Nature*, **437**, 400–403, https://doi.org/10.1038/nature03936.

——, L. F. Kilcher, and J. N. Moum, 2009: Structure and composition of a strongly stratified, tidally pulsed river plume. *J. Geophys. Res.*, **114**, C00B12, https://doi.org/10.1029/2008JC005036.

Olabarrieta, M., W. R. Geyer, and N. Kumar, 2014: The role of morphology and wave-current interaction at tidal inlets: An idealized modeling analysis. *J. Geophys. Res. Oceans*, **119**, 8818–8837, https://doi.org/10.1002/2014JC010191.

Peregrine, D. H., 1998: Surf zone currents. *Theor. Comput. Fluid Dyn.*, **10**, 295–309, https://doi.org/10.1007/s001620050065.

Raubenheimer, B., R. T. Guza, and S. Elgar, 1996: Wave transformation across the inner surf zone. *J. Geophys. Res.*, **101**, 25 589–25 597, https://doi.org/10.1029/96JC02433.

Rehmann, C. R., 2004: Scaling for the mixing efficiency of stratified grid turbulence. *J. Hydraul. Res.*, **42**, 35–42, https://doi.org/10.1080/00221686.2004.9641181.

Reniers, A. J. H. M., J. H. MacMahan, E. B. Thornton, T. P. Stanton, M. Henriquez, J. W. Brown, J. A. Brown, and E. Gallagher, 2009: Surf zone surface retention on a rip-channeled beach. *J. Geophys. Res.*, **114**, C10010, https://doi.org/10.1029/2008JC005153.

Rodriguez, A. R., S. N. Giddings, and N. Kumar, 2018: Impacts of nearshore wave-current interaction on transport and mixing of small-scale buoyant plumes. *Geophys. Res. Lett.*, **45**, 8379–8389, https://doi.org/10.1029/2018GL078328.

Spydell, M. S., and F. Feddersen, 2009: Lagrangian drifter dispersion in the surf zone: Directionally spread normally incident waves. *J. Phys. Oceanogr.*, **39**, 809–830, https://doi.org/10.1175/2008JPO3892.1.

——, and ——, 2012: A Lagrangian stochastic model of surf zone drifter dispersion. *J. Geophys. Res.*, **117**, C03041, https://doi.org/10.1029/2011JC007701.

——, ——, R. T. Guza, and W. E. Schmidt, 2007: Observing surf-zone dispersion with drifters. *J. Phys. Oceanogr.*, **37**, 2920–2939, https://doi.org/10.1175/2007JPO3580.1.

Stacey, M. T., and D. K. Ralston, 2005: The scaling and structure of the estuarine bottom boundary layer. *J. Phys. Oceanogr.*, **35**, 55–71, https://doi.org/10.1175/JPO-2672.1.

Stretch, D. D., J. W. Rottman, S. K. Venayagamoorthy, K. K. Nomura, and C. R. Rehmann, 2010: Mixing efficiency in decaying stably stratified turbulence. *Dyn. Atmos. Oceans*, **49**, 25–36, https://doi.org/10.1016/j.dynatmoce.2008.11.002.

Terray, E. A., M. A. Donelan, Y. C. Agrawal, W. M. Drennan, K. K. Kahma, A. J. Williams, P. A. Hwang, and S. A. Kitaigorodskii, 1996: Estimates of kinetic energy dissipation under breaking waves. *J. Phys. Oceanogr.*, **26**, 792–807, https://doi.org/10.1175/1520-0485(1996)026<0792:EOKEDU>2.0.CO;2.

Thomson, J., 2012: Wave breaking dissipation observed with SWIFT drifters. *J. Atmos. Oceanic Technol.*, **29**, 1866–1882, https://doi.org/10.1175/JTECH-D-12-00018.1.

——, A. R. Horner-Devine, S. Zippel, C. Rusch, and W. Geyer, 2014: Wave breaking turbulence at the offshore front of the Columbia River plume. *Geophys. Res. Lett.*, **41**, 8987–8993, https://doi.org/10.1002/2014GL062274.

——, and Coauthors, 2019: A new version of the swift platform for waves, currents, and turbulence in the ocean surface layer. *2019 IEEE/OES Twelfth Current, Waves, and Turbulence Measurement and Applications Workshop*, San Diego, CA, Institute of Electrical and Electronics Engineers, 1–7, https://doi.org/10.1109/CWTM43797.2019.8955299.

Thornton, E. B., and R. T. Guza, 1983: Transformation of wave height distribution. *J. Geophys. Res.*, **88**, 5925–5938, https://doi.org/10.1029/JC088iC10p05925.

——, and ——, 1986: Surf zone longshore currents and random waves: Field data and models. *J. Phys. Oceanogr.*, **16**, 1165–1178, https://doi.org/10.1175/1520-0485(1986)016<1165:SZLCAR>2.0.CO;2.

Thorpe, S. A., 1973: Turbulence in stably stratified fluids: A review of laboratory experiments. *Bound.-Layer Meteor.*, **5**, 95–119, https://doi.org/10.1007/BF02188314.

Turner, J. S., 1973: *Buoyancy Effects in Fluids*. Cambridge University Press, 368 pp.

White, H., 1980: A heteroskedasticity-consistent covariance matrix and a direct test for heteroskedasticity. *Econometrica*, **48**, 817–838, https://doi.org/10.2307/1912934.

Wong, S. H. C., S. G. Monismith, and A. B. Boehm, 2013: Simple estimate of entrainment rate of pollutants from a coastal discharge into the surf zone. *Environ. Sci. Technol.*, **47**, 11 554–11 561, https://doi.org/10.1021/es402492f.

Wright, L. D., R. T. Guza, and A. D. Short, 1982: Dynamics of a high-energy dissipative surf zone. *Mar. Geol.*, **45**, 41–62, https://doi.org/10.1016/0025-3227(82)90179-7.

Zippel, S., and J. Thomson, 2015: Wave breaking and turbulence at a tidal inlet. *J. Geophys. Res. Oceans*, **120**, 1016–1031, https://doi.org/10.1002/2014JC010025.

——, and ——, 2017: Surface wave breaking over sheared currents: Observations from the mouth of the Columbia River. *J. Geophys. Res. Oceans*, **122**, 3311–3328, https://doi.org/10.1002/2016JC012498.